University of Pittsburgh

Annual Progress Report: 2011 Formula Grant

Reporting Period

July 1, 2013 – June 30, 2014

Formula Grant Overview

The University of Pittsburgh received $7,809,060 in formula funds for the grant award period January 1, 2012 through December 31, 2015. Accomplishments for the reporting period are described below.

Research Project 1: Project Title and Purpose

Research Infrastructure: Structural Biology Renovations – The purpose of this project is to renovate two areas of the University of Pittsburgh's Biomedical Science Tower 3 (BST3) to meet the evolving needs of the Department of Structural Biology and to alleviate overcrowding among all departments housed in BST3.

Duration of Project

1/1/2012 – 6/30/2013

Summary of Research Completed

This project ended during a prior state fiscal year. For additional information, please refer to the Commonwealth Universal Research Enhancement C.U.R.E. Annual Reports on the Department's Tobacco Settlement/Act 77 web page at http://www.health.state.pa.us/cure.

Research Project 2: Project Title and Purpose

Thermodynamic Studies of Ligand Binding – Advances in the development of predictive levels of understanding of biological processes at a systems level as well as the development of methods for the design of molecules that can perturb biological systems, including drugs, depends on a thorough understanding of the physical parameters associated with the interactions between biological molecules, including binding affinities. This project aims to complement ongoing activities in structural biology, molecular biophysics, computational chemistry, and systems biology at the University of Pittsburgh.

Anticipated Duration of Project

1/1/2012 – 6/30/2015

Project Overview

All biological processes depend on interactions between sets of macromolecules. Thus, the development of a deep understanding of such interactions is an important goal. One key area in which such understanding is sought is the prediction of binding affinity for interacting pairs of molecules given the three-dimensional structure of the complex between these molecules.

A useful system for developing such methods is a peptide-binding system associated with the targeting of proteins to peroxisomes in eukaryotic cells. This system consists of the protein Pex5p and peptides containing type 1 peroxisome targeting signals (PTS1). Structures are known for the PTS1-binding domain from human Pex5p, both in the presence and absence of bound ligands. Moreover, the binding of a range of PTS1 peptides has been examined, and these peptides bind with a wide range of affinities.

A systematic study of the binding affinities of a series of PTS1 peptides with variations in the amino acid sequence will be conducted. Initial studies will focus on the PTS1 peptides related to the sequence TyrLysGlyGlyLysSerLysLeu-COO^- since this sequence has been the basis for many cell biological studies. The binding affinities and corresponding binding free energies will be determined for a series of peptides with one or two amino acids within this sequence changed from the parent peptide. The results of these studies will be used to develop computational approaches that are intended to allow the prediction of binding affinity from amino acid sequence for a larger series of PTS1 peptides. In addition, some of these binding affinities will be dissected into their thermodynamic components through the use of isothermal titration calorimetry. The data sets developed will be used to test and refine the methods for predicting binding affinity and other thermodynamic parameters.

Principal Investigator

Jeremy M. Berg, PhD
Professor, Computational and Systems Biology
University of Pittsburgh
Scaife Hall, S304
3550 Terrace Street
Pittsburgh, PA 15261

Other Participating Researchers

None

Expected Research Outcomes and Benefits

The affinities (and associated standard free energies of binding) of a series of peptides containing type 1 peroxisome targeting signals for the human peroxisome targeting receptor Pex5p will be determined. These peptides will be designed to have both single and double amino acid substitutions from a known peroxisomal targeting sequence. For a selected set of these peptides, the binding free energies will be dissected into their enthalpic and entropic components through

the use of isothermal titration calorimetry. The results from these studies will be used to develop computational models that enable the calculation of thermodynamic parameters for the binding of a larger series of peroxisomal targeting peptides to Pex5p. These computational models will be used to understand the binding and targeting properties of peroxisomal proteins and enzymes, enabling systems-wide analysis of this fundamental biological process. This approach has the potential to be generalized for use in the understanding of other protein-peptide and protein-protein interaction networks. The development of such methods will enable computational modeling of important biochemical networks to facilitate a predictive level of understanding of these systems in health and disease. Furthermore, the insights generated may be of use for the analysis of other macromolecular interactions, including those between drugs and their targets.

Summary of Research Completed

To complement the experimental studies of binding free energy for a series of PTS1 peptides, I have initiated computational studies to calculate the relative binding free energies for a series of peptides from physical principles based on their three-dimensional structures. These calculations use the three-dimensional structure of a previously determined Pex5p-PTS1 peptide complex and are based on so-called free energy perturbation methods. Briefly, these methods allow one amino acid to be computationally converted to another amino acid within the protein-peptide complex and the associated free energy change to be estimated through molecular dynamics-based sampling. The conversion of one amino acid to another takes place in a number of steps corresponding to nonphysical hybrid amino acids to allow the changes to be small enough to allow adequate sampling of configurations within an equilibrium distribution.

As an initial project for these methods, I examined the relative binding free energies of the PTS1 peptide Tyr-Gln-Ser-Lys-Leu (which was used in the determination of the three-dimensional structure of the Pex5p-PTS1 peptide complex) and Tyr-Gln-Ser-Lys-Ile. The process proceeded as follows:

(1) The structure of the Pex5p-PTS1 peptide complex was modified by filling in loops that were not visible in the crystal structure through an automated procedure based on identifying loops of similar amino acid sequences in other proteins. None of these loops were close to the PTS1 peptide-binding site so these modifications were not likely to have significant effects, but the loop closure eliminates any concern about nonphysical structural changes occurring during the molecular dynamics calculations.
(2) The complex structure was computationally embedded in a box of water molecules with Na^+ and Cl^- ions added to neutralize the structure and generate an NaCl concentration of approximately 0.15M, corresponding to the conditions used for the experimental peptide binding studies. These and all subsequent calculations were performed with the public domain molecular dynamics and analysis program VMD.
(3) The initial Tyr-Gln-Ser-Lys-Leu complex was equilibrated using molecular dynamics.
(4) The Leu side chain was converted to Ile in approximately 40 steps, with 500 picoseconds of molecular dynamics at each step used to estimate the free energy change associated with each step.
(5) The overall free energy change was calculated by summing the estimated free energy changes for each step.

(6) The process was repeated for the conversion in reverse (from Ile to Leu) to check whether the results are comparable and allow error estimation.

These calculations revealed a free energy difference between the Tyr-Gln-Ser-Lys-Leu and Tyr-Gln-Ser-Lys-Ile of 22.6 ± 0.5 kcal/mol.

This free energy difference must be compared with the free energy differences for interconverting these two peptides free in solution rather than in the context of the Pex5p complex. The calculations above were repeated for the free peptides in boxes of water with 0.15 M NaCl. This process revealed a free energy difference of 20.7 ± 0.2 kcal/mol. Taken together with the results for the complexes, the calculations predict that the Tyr-Gln-Ser-Lys-Leu peptide should bind (22.6 -20.7) = 1.9 kcal/mol with an uncertainty of approximately 0.6 kcal/mol. This can be compared with an experimental difference of 2.3 ± 0.2 kcal/mol. The reasonable agreement between the computed value and the experimental value provided support for the proposal to extend these computational studies to other peptides.

Additional calculations have been performed for Tyr-Gln-Ser-Lys-Met, Tyr-Gln-Ser-Lys-Phe, and Tyr-Gln-Ser-Lys-Ala. Results from these calculations are compared with the experimental values in Figure 1.

Reasonable agreement is observed between the calculated and experimental results, with some significant differences that will be investigated through additional calculations. These studies will also be extended to variations in other positions within the PTS1 peptide sequence.

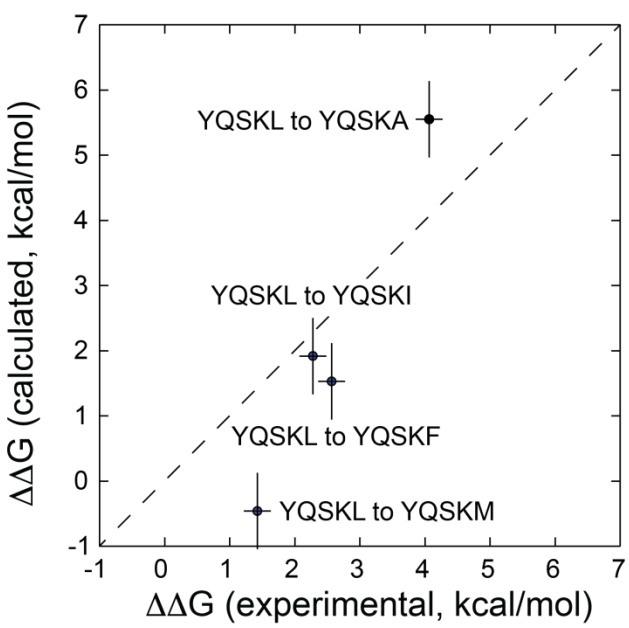

Figure 1. A comparison between calculated and experimental relative binding free energies for a series of PTS1 peptides with variations in the carboxyl-terminal position. The dotted line has slope 1 (corresponding to perfect agreement between calculated and experimental results and has not been fit to the data).

Research Project 3: Project Title and Purpose

Neurobiology of Addiction – Substance use disorders and addiction are major public health problems, yet few effective treatments or preventions exist. Recent advances in understanding the factors associated with increased risk for addiction (e.g., alterations in circadian rhythms) and in the neuroscience of reward-related circuitry make it possible to take new approaches to understanding the neurobiology of addiction and, thus, enhance our capacity to develop novel preemptive interventions. We propose three aims that will address key issues in the neurobiology of addiction.

Anticipated Duration of Project

1/1/2012 – 12/31/2015

Project Overview

We will investigate three specific aims to address the neurobiological causes and consequences of substance abuse. The studies focus on cocaine abuse, but the results will be widely informative to multiple forms of addiction. The first aim will examine how patterns of gene expression in the nucleus accumbens (NAc), a key node in the circuitry of the brain that mediates rewarding experiences, are regulated by genes that control circadian rhythms and how cocaine administration alters these patterns. The second aim will determine whether chronic cocaine self-administration in macaque monkeys results in structural alterations similar to those that accompany cognitive deficits in human cocaine users. The third aim will determine how sleep deprivation can alter neuronal function in the NAc, so as to increase the susceptibility of the brain's reward circuitry to the addictive effects of cocaine. Thus, these studies involve an integration of genetic, molecular, imaging, and electrophysiological investigations in mice and monkeys that will provide new insights into the factors that increase the risk for cocaine addiction and alter brain circuitry in a way that sustains addictive behaviors.

Principal Investigator

David A. Lewis, MD
Professor and Chair of Psychiatry; Director, Translational Neuroscience Program
Medical Director, Western Psychiatric Institute and Clinic
University of Pittsburgh
Thomas Detre Hall
3811 O'Hara Street
Pittsburgh, PA 15213

Other Participating Researchers

Yanhua Huang, PhD; Mary Torregrossa, PhD– employed by the University of Pittsburgh

Expected Research Outcomes and Benefits

An increasing body of evidence suggests that genes controlling circadian rhythms are also involved in modulating the addictive properties of drugs of abuse. Indeed, drug addiction is associated with major disruptions in the sleep/wake cycle. Specific Aim 1 will determine (1) whether genetic disruptions to the circadian clock increase the risk for drug addiction and (2) whether drugs of abuse can entrain circadian gene expression in the NAc, leading to increased craving or drug seeking at the time of day that drug use normally occurs. Cocaine dependence is also characterized by an inability of individuals to make appropriate choices between incentives of drug use versus the everyday incentives of work and family. Clinical studies of drug users indicate a pattern of cognitive deficits manifested at the levels of inhibitory control and executive functioning. However, few studies have examined the cellular basis of altered inhibitory control and cognition in cocaine dependence using clinically relevant animal models in a manner that controls for factors that pre-exist drug use in humans. Specific Aim 2 will resolve the role of cocaine use (as opposed to pre-existing conditions) in generating structural brain abnormalities and determine how those structural changes relate to altered impulsivity. Sleep abnormalities may not only be a symptom, but also a causal factor, for addiction. On one hand, acute sleep disturbance is triggered by cocaine use. On the other hand, people with insomnia are more prone to developing addiction. The reciprocally promoting effects between sleep disorders and drug abuse suggest a common neural basis. Specific Aim 3 will determine whether sleep deprivation can predispose the brain's reward circuitry to addiction by altering the membrane properties and synaptic transmission of NAc neurons.

Summary of Research Completed

<u>Aim 1—Mary Torregrossa, PhD</u>
The overall goal of Aim 1 is to examine how patterns of gene expression in the nucleus accumbens (NAc), a key node in the circuitry of the brain that mediates rewarding experiences, are regulated by genes that control circadian rhythms and how cocaine administration alters these patterns. To address this aim, the Torregrossa lab focuses on understanding factors that underlie risk-versus-resilience for the development of addictive disorders. Because stress during adolescence increases substance use risk, the Torregrossa team seeks to first characterize these age-dependent effects on the relevant brain circuitry.

Studies and Results
During the reporting period, we have made significant progress in accomplishing our experimental goals; our specific achievements related to Aim 1 are listed below by individual goals:

Goal 1. Adolescence is known to be a time of ongoing brain development and enhanced vulnerability to addictive disorders. Some clinical studies suggest that highly stressful adolescent experiences increase risk for developing addictive disorders—independent of the particular substance used—in adulthood. We have piloted these investigations in our rat model (see also Goal 2) with alcohol rather than cocaine because alcohol is easier to use. For example, we previously found that in male rats, adolescent exposure to high levels of the glucocorticoid stress hormone, corticosterone (CORT), led to an increased motivation for and self-administration of

alcohol in adulthood. We wanted to expand these studies to determine whether (1) similar effects occurred in female rats and (2) adolescent social isolation stress (SIS) could recapitulate the effects of chronic CORT exposure. We examined a variety of alcohol-motivated animal behaviors, including operant self-administration and relapse-like behavior induced by cues or a pharmacological stressor. In summary, there is a general trend for adolescent CORT exposure to enhance self-administration and consumption of alcohol in female rats. Females also show greater self-administration and consumption of alcohol than males (Fig. 1A-B). In addition, females reinstate (i.e., relapse) more in response to cues and pharmacological stress than males, with adolescent females exposed to CORT demonstrating the most robust reinstatement responses (Fig. 1C-D). In studies we have conducted to date, adolescent rats exposed to SIS do not show a difference in alcohol-motivated behaviors (as we had expected based on previous studies in the literature). However, we conducted intermediate anhedonia and anxiety testing that may have influenced our results.

Goal 2. Previously, we attempted to determine the mechanism underlying the increased motivation for alcohol induced by adolescent CORT exposure. We performed proteomics analysis of specific brain regions, looking for changes in the signaling of molecules that persist into adulthood after CORT exposure in rats. One of the differentially regulated proteins identified in the amygdala was the alpha2a-adrenergic receptor (a2AR), which showed an increase in phosphorylation at sites regulated by the G-protein coupled receptor kinase 2 (GRK2). The a2AR is a critical regulator of norepinephrine (NE) signaling in the amygdala; and a decrease in a2AR function can result in enhanced NE release, enhanced anxiety, and, potentially, motivation for alcohol. Phosphorylation of a2ARs by GRK2 promotes desensitization and internalization of the receptor, resulting in reduced receptor function and an overall increase in NE signaling. Thus, in the past year of funding, we conducted studies to determine whether inhibiting GRK2 in the amygdala in rats could reduce motivation for and relapse to alcohol-seeking at baseline and in response to a pharmacological stressor (yohimbine). Figure 3 illustrates the results, showing a robust reduction in yohimbine-induced motivation for alcohol (Fig. 2A) and reinstatement (Fig. 2B). In some cases, it appears that a GRK2 inhibitor can also reduce baseline responses for alcohol and can reduce impulsivity (data not shown). Therefore, GRK2 inhibition may represent a novel mechanism for the treatment of alcohol use disorders (AUDs), particularly alcohol drinking motivated by stress.

Goal 3. One known way to treat addictive disorders, like cocaine use, is to reduce the strength of memories associated with drug use, because these maladaptive memories drive continued use and relapse after abstinence. In humans, drug memories can be weakened either by preventing reconsolidation of the memories into long-term storage after reactivation or by extinguishing the memory by repeatedly presenting drug-associated cues in the drug's absence. Reconsolidation can be disrupted, and extinction enhanced, by pharmacological manipulations; however, there is a need to identify the cellular and molecular mechanisms that regulate these learning processes so that more effective and specific therapeutic agents can be developed as addiction treatments. Using a rat model, we performed phosphoproteomic analysis of the amygdala to identify the molecular mechanisms that regulate drug memories.

We sought to identify signaling cascades that were specifically engaged when a cocaine-associated memory was reactivated and reconsolidated, versus extinguished, relative to control

rats. One of the identified molecules that showed differential regulation under extinction and reconsolidation conditions was Ca2+-calmodulin dependent kinase IIa (CaMKIIa). CaMKIIa was differentially phosphorylated on serine 331 (S331), with an increase in phosphorylation in the extinction condition and a decrease in the reconsolidation condition. Unfortunately, the function of phosphorylation at this site is not currently known. In ongoing experiments, we are mutating S331 of CaMKIIa to make the protein either non-phosphorylatable or constitutively phosphorylated, and we are determining the effects of these mutations on enzyme function and on the structure of dendritic spines.

In addition, we have tested the ability of a CaMKII inhibitor to regulate extinction and reconsolidation of cocaine-cue memories when infused into the basolateral amygdala. Interestingly, we have found that the inhibitor (KN62) can dose-dependently facilitate extinction of cocaine-cue memories with moderate levels of cue exposure (extinction training). KN62 also moderately inhibits memory reconsolidation, resulting in reduced reinstatement to cocaine seeking in rats (Fig. 3). Therefore, inhibition of CaMKII represents a potential therapeutic approach for disrupting cocaine-associated memories to reduce relapse.

Goal 4. In addition to CaMKIIa, several other protein-signaling cascades have the potential to regulate cocaine-associated memories and may, simultaneously, inhibit reconsolidation and enhance extinction to robustly weaken drug memory. Our proteomics analysis, described above, identified connexin 43, an astrocytic gap junction protein, as one such target. Moreover, the transcription factor, nuclear factor kappa B (NFkB) has also been implicated in bidirectional memory regulation in fear-conditioning studies.

We attempted to inhibit reconsolidation of cocaine-cue memories in rats by manipulating these proteins with pharmacological agents in the amygdala. Unfortunately, manipulations of these signaling cascades after cocaine memory reactivation did not reduce reinstatement of drug seeking (data not shown).

Significance
These experiments in rats are identifying novel signaling cascades involved in the extinction and reconsolidation of drug-associated memories and testing the capability of manipulations of molecules to prevent relapse in a preclinical animal model. Once we identify the molecular underpinnings of these memory processes, we will be better able to identify novel pharmacotherapies that may serve as adjuncts to exposure therapy in treating cocaine use and addiction to other substances. For example, our findings continue to progress toward identifying novel signaling cascades that may serve as treatment development targets, including inhibition of c-Jun N-terminal kinase 3 (JNK3), a protein kinase that is already a basis of medication development for other indications.

<u>Aim 2—Tobias Teichert, PhD</u>
Aim 2 will determine whether chronic cocaine self-administration in macaque monkeys results in structural brain alterations similar to those that accompany cognitive deficits in human cocaine users. Interpreting the functional significance of, and the potential mechanism underlying, changes in brain structure in association with cannabis use requires a means to index the network properties of neural circuits in the altered brain regions. Toward that end, efforts since the

appointment of Dr. Teichert to the faculty 10 months ago have been directed at building an electroencephalograph (EEG) set-up for nonhuman primates to record auditory evoked potentials in an oddball task.

The main dependent variable is the so-called auditory mismatch-negativity (aMMN), a fronto-central negative event-related potential (ERP) that peaks between 100 and 150 milliseconds after the onset of a deviant tone. The aMMN is a marker of preconscious auditory processing that may direct attention to specific sounds that signal change in the auditory environment. It is an important first processing step for high level auditory processing of this stimulus.

In humans, deficits in auditory mismatch negativity have been linked to impaired speech comprehension, ability to recognize auditory emotional cues, and social cognition. Mismatch negativity is affected in addictive disorders and other psychiatric conditions. The mechanisms by which cocaine or other addictive substances affect aMMN are still a matter of debate, however. Our studies will help understand aMMN pathways, how they may be affected in addiction, and, ultimately, how they are related to structural changes in the relevant brain regions. The progress report will be divided into two parts: (1) issues related to purchasing and training of nonhuman primates; and (2) issues related to the lab setup.

(1) Nonhuman primates
Purchasing. The lab has purchased five animals. Four are young male rhesus macaques (4-5 years old, 7-9 kg) purchased from the University of California, Davis (UC-Davis). The animals came out of quarantine at the beginning of May 2014 without any identified health concerns. A fifth animal, which had previously been used as a control subject in a cocaine study, was purchased from a primate lab at the University of Pittsburgh (10 years old, 11 kg). This fifth animal will be used as a pilot animal to optimize procedures for the four experimental animals.

Magnetic resonance (MR) and computed tomography (CT) imaging. All four animals from UC-Davis were imaged to assure normal brain anatomy. On May 8, 2014, we performed the MR imaging and collected 3 T1-weighted high-resolution structural scans. In addition, we collected a T2 weighted scan and a diffusion weighted scan. T1 images were aligned and averaged to achieve better signal-to-noise ratio. Images were taken while the animals were positioned in an MR compatible stereotax. Hence, images were already very closely in line with a stereotactic coordinate system. Using off-line realignment tools, we corrected for small deviations to achieve the best possible match to the stereotactic coordinate system.

On June 25, 2014, we recorded CT images from the four UC-Davis animals. The axial resolution of the scanner is 1.25 mm. From each animal, we collected one axial and one coronal image. We then registered the two images to the MR-based stereotactic coordinate system with isotropic voxel resolution of 0.5 mm^3. By averaging the two images from the two different orientations, we minimized the impact of the low axial resolution of the CT scans.

Training. The older animal was already chair-trained by the time he arrived in the lab. The animal is currently in pen housing, and we successfully familiarized him with the system that we use to get the animals from a pen to a smaller transport cage. The four new animals are currently housed in individual cages and were trained to climb from cage to primate chair. The animals

were also familiarized with the lab recording chamber.
(2) Lab setup
Primate chairs. We have purchased one primate chair and ordered a second from Scientific Design.

Recording booth. The lab was able to obtain a used electrically and acoustically shielded recording chamber from the recently closed lab of Herbert Terrace, PhD, at Columbia University. We have built a new aluminum back wall into the chamber with a Plexiglas window, behind which a light-emitting diode (LED) monitor is mounted. The wall also has two nubs that serve to position the primate chair.

Stimulus presentation. Experimental control is handled by a Windows PC running an in-house modified version of the *matlab* toolbox *monkeylogic*. Sound generation is handled by a sub-routine of the *matlab* toolbox *Psychtoolbox*, in combination with an M-192 sound card (M-Audiophile, 48KHz) and sent to a set of stereo speakers (Manger Schallwandler). The timing of sound presentation on Windows machines is typically very unreliable. However, using this setup, we can achieve presentation accuracy of ±0.5 milliseconds. This accuracy is more than enough for our main purpose of recording long-latency cortical auditory potentials. In addition, we can record the actual sound onset by using a microphone. This process enables us to identify sound onset and realign data to sound onset with an accuracy determined by the sampling rate of the recording system (up to 30 kHz; see below).

Monkeylogic system timing is linked to the vertical refresh rate of the attached monitor. Sound onset can be timed to coincide with a visual prompt or to precede/lag the visual stimulus by an arbitrary amount. This process allows us to closely coordinate audiovisual events with continuous stimulus onset asynchrony. *Monkeylogic* is also capable of monitoring animal behavior (eye movements or button presses) and triggering short latency-contingent stimuli or other changes in experimental flow. For the passive auditory stimulation paradigms that we will use initially, this is not necessary.

Recording setup. For recording purposes, the lab purchased the Intan digital recording system RHD2000. The Intan system has a sampling rate between 1 and 30 kHz and a noise floor of ~20μV and a 256-channel recording capacity. Currently, the lab has one 64-channel and one 32-channel amplifier board, for a total of 96 simultaneously recorded unipolar channels. In addition, the system has eight onboard analog and 16 onboard digital channels. The digital ports have been set up to record trial condition information from the *monkeylogic* stimulus presentation system, which are delivered as a continuous 8-bit digital code. One of the analog channels records data from the microphone to allow an offline realignment of EEG traces to stimulus onset. A second channel captures output from a short latency photo diode placed in the corner of the monitor to record the appearance of a visual synchronization signal.

We are testing a low-noise EEG system (36-channel 5kHz EEG amplifier from Brain Products). If the Brain Products amplifier provides significantly better recordings, we will purchase the EEG amp and run it in parallel to the Intan system. The Intan system, with its higher temporal resolution, will then serve as a master system.

Aim 3—Yanhua Huang, PhD

Specific Aim 3 will determine whether sleep deprivation can predispose the brain's reward circuitry to addiction by altering the membrane properties and synaptic transmission of NAc neurons.

Goal 1. Determine whether poor-quality sleep as a consequence of drug use exacerbates addiction-related behaviors during abstinence and whether sleep interventions could alleviate symptoms.

Goal 2. Determine whether and how sleep deprivation regulates the neural activity of the nucleus accumbens, a critical brain region that regulates motivational drives and reward-seeking behaviors.

(1) Sleep regulates incubation of cocaine craving in rats.

Human and animal studies suggest that sleep quality deteriorates during long-term abstinence from repeated use of addictive drugs like cocaine. Poor sleep quality has been thought to contribute to relapse, mainly based on correlation analysis in humans and sleep deprivation studies in animals. However, sleep deprivation is different from insomnia; thus, it remains unclear whether poor sleep attributable to drug use exacerbates addiction-related behaviors during abstinence, or whether sleep interventions could alleviate symptoms. We use a cocaine self-administration (SA) model in rats to examine this question using a multidisciplinary approach, including *in vitro* brain slice electrophysiology, *in vivo* EEG recordings, sleep intervention, and behavioral tests of cocaine craving incubation (time-dependent increases in cocaine seeking after withdrawal). Following cocaine SA training (2 hr/d x 5 d) in young adult rats (P37-41 at start of training), rats underwent withdrawal in their home cages while EEG and electromyography (EMG) signals were chronically recorded. Compared to baselines (recorded prior to cocaine exposure), both non-rapid eye movement (NREM) and rapid eye movement (REM) total sleep times were reduced during withdrawal day 1 through three weeks. Recovery trends were observed from weeks 4 to 6. NREM and REM episode durations were reduced in the light phase during long-term withdrawal. To enhance the consolidated sleep in the light phase, we used a custom-made treadmill system to sleep deprive the rats, without significant exercise, during the dark phase only. All animals were trained and tested during the dark phase and allowed three manipulation-free days following sleep interventions before any behavioral tests. We observed that 6-week, or 3-week (but not 1- or 2-week), sleep interventions toward the end of the withdrawal period significantly reduced cue-induced cocaine seeking, without significantly affecting natural reward-associated learning (sucrose SA).

Electrophysiology (E-phys) recordings of *in vitro* brain slices revealed that the 3-week sleep intervention significantly reduced the synaptic content of calcium-permeable AMPA receptors (CP-AMPARs) in nucleus accumbens medium spiny neurons, which has been shown at these synapses to critically regulate incubation of cocaine craving following long-term withdrawal. By contrast, sleep fragmentation at 3 weeks significantly enhanced the synaptic level of CP-AMPARs, as well as cue-induced cocaine seeking. Thus, sleep could bi-directionally regulate addiction-associated behaviors during abstinence, with corresponding changes in the neurophysiology within the nucleus accumbens. A manuscript is being prepared.

(2) Sleep regulates nucleus accumbens neurons.

Sleep disturbance disrupts physiological homeostasis and is a potent pathogenic factor for a variety of psychiatric diseases, although the underlying neural basis remains elusive. We have been focusing on whether and how sleep deprivation regulates the neural activity of the nucleus accumbens, a critical brain region in regulating motivational drives and reward-seeking behaviors. Thus far, we have determined:

- Acute sleep deprivation led to enhanced sucrose self-administration in mice.
- Acute sleep deprivation reduced the excitatory/inhibitory synaptic transmission (E/I) ratio in the accumbens principal neurons.
- Reduced probability of glutamate release in the accumbens contributed to a decrease in the E/I ratio.
- Reduction of glutamate release probability was specific to the basal lateral amygdala and medial prefrontal cortex-to-accumbens pathways, but not the hippocampal or thalamic projections.
- Blocking adenosine receptors could restore glutamate release and E/I ratio in the accumbens following acute sleep deprivation.
- Selective block of adenosine A1 and A2a receptors within the accumbens immediately following sleep deprivation restored a normal level of sucrose self-administration in mice.

(3) Dopamine released at the ventral tegmental area (VTA)-to-accumbens projection terminals triggers long-term depression at heterosynaptic GABAergic synapses. This plasticity is negated after withdrawal from cocaine exposure.

(4) Following long-term withdrawal from self-administered cocaine, nucleus accumbens neurons exhibit sustained reduction of unitary inhibitory transmissions, as well as enhanced excitation/inhibition ratio; the changes are temporarily relieved with cocaine re-exposure after long-term withdrawal.

(5) Following long-term withdrawal from cocaine self-administration in rats, synaptic insertion of calcium-permeable AMPA receptors (CP-AMPARs) occurs at amygdala-to-nucleus accumbens (NAc) synapses. This activity is thought to mediate the maturation of silent synapses, which are induced by repeated cocaine exposure and express NMDA- but not AMPA-type glutamate receptors. *In vivo* optogenetic stimulation-induced downregulation of CP-AMPARs at amygdala-to-NAc synapses, which re-silenced some of the previously silent synapses after prolonged withdrawal, decreased cocaine craving incubation. Our findings indicate that silent synapse-based reorganization of the amygdala-to-NAc projection is critical for persistent cocaine craving and relapse after withdrawal.

Ishikawa M, Otaka M, Huang YH, Neumann PA, Winters BD, Grace AA, Schlüter OM, Dong Y (2013) Dopamine triggers heterosynaptic plasticity. *J Neurosci* 33:6759-6765.

Otaka M, Ishikawa M, Lee BR, Liu L, Neumann PA, Cui R, Huang YH, Schlüter OM, and Dong Y (2013) Exposure to Cocaine Regulates Inhibitory Synaptic Transmission in the Nucleus Accumbens. *J Neurosci* 33:6753-6758.

Chen B, Wang Y, Ma Y, Wang X, Schlüter OM, Dong Y, Huang YH (2013) Cocaine-induced Membrane Adaptation in the Central Nucleus of Amygdala. *Neuropsychopharmacology* 38:2240-2248.

Ishikawa M, Otaka M, Neumann PA, Wang Z, Cook JM, Schlüter OM, Dong Y, Huang YH (2013) Exposure to cocaine regulates inhibitory synaptic transmission from the ventral tegmental area to the nucleus accumbens. *J Physiol* 591:4827-4841.

Lee BR, Ma YY, Huang YH, Wang X, Otaka M, Ishikawa M, Neumann PA, Graziane NM, Brown TE, Suska A, Guo C, Lobo MK, Sesack SR, Wolf ME, Nestler EJ, Shaham Y, Schlüter OM, Dong Y (2013) Maturation of silent synapses in amygdala-accumbens projection contributes to incubation of cocaine craving. *Nat Neurosci* 16:1644-1651.

Krueger JM, Huang YH, Rector DM, Buysse DJ (2013) Sleep: a synchrony of cell activity-driven small network states. *Eur J Neurosci* 38:2199-2209.

Huang YH, Schlüter OM, Dong Y (2013) An unusual suspect in cocaine addiction. *Neuron* 80:835-836.

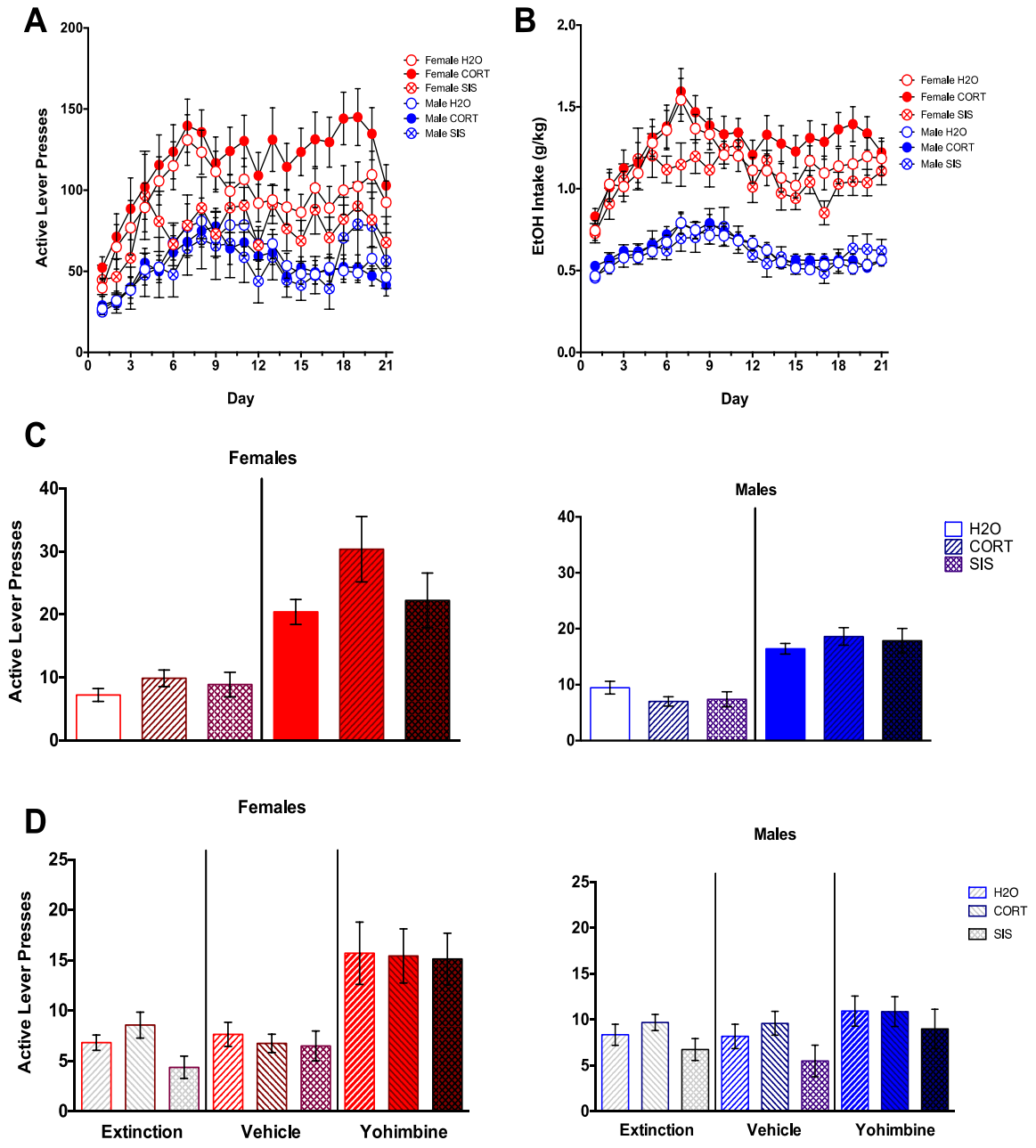

Figure 1**.** Adolescent CORT, but not social isolation stress, increases responding for alcohol (A) and total consumption (B), particularly in female rats. Females also respond more and consume more alcohol than males. Likewise, females reinstate more to alcohol cues than males (C), with adolescent CORT exposure enhancing cue-induced reinstatement. Females reinstate more to the pharmacological stressor yohimbine and are more sensitive to lower doses of yohimbine than males (D). N=8/group.

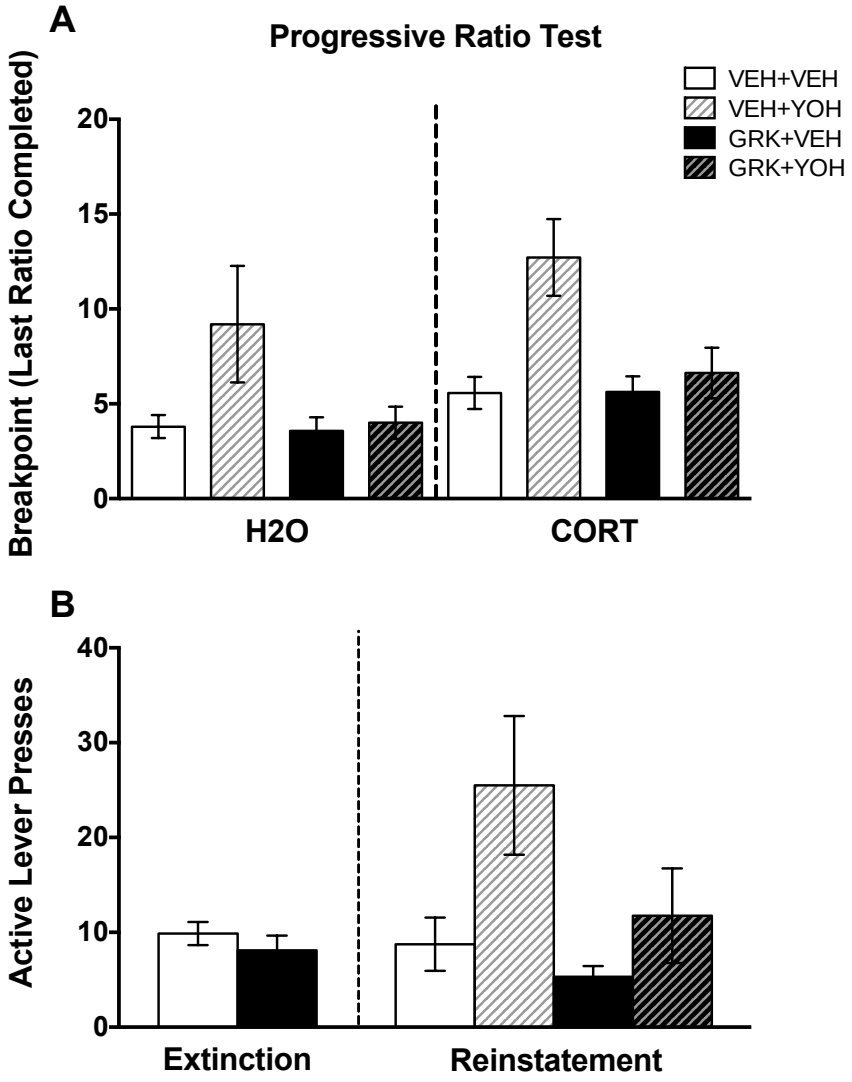

Figure 2. Adolescent CORT-exposed rats demonstrate greater motivation for alcohol on a progressive ratio test, and the pharmacological stressor yohimbine further increases motivation for alcohol in both groups. Intra-amygdala administration of a GRK2 inhibitory peptide had no effect on its own, but significantly reduced yohimbine-induced alcohol responding (A). The GRK2 inhibitor was also able to significantly reduce reinstatement to alcohol-seeking induced by yohimbine (B). N=7-8/group.

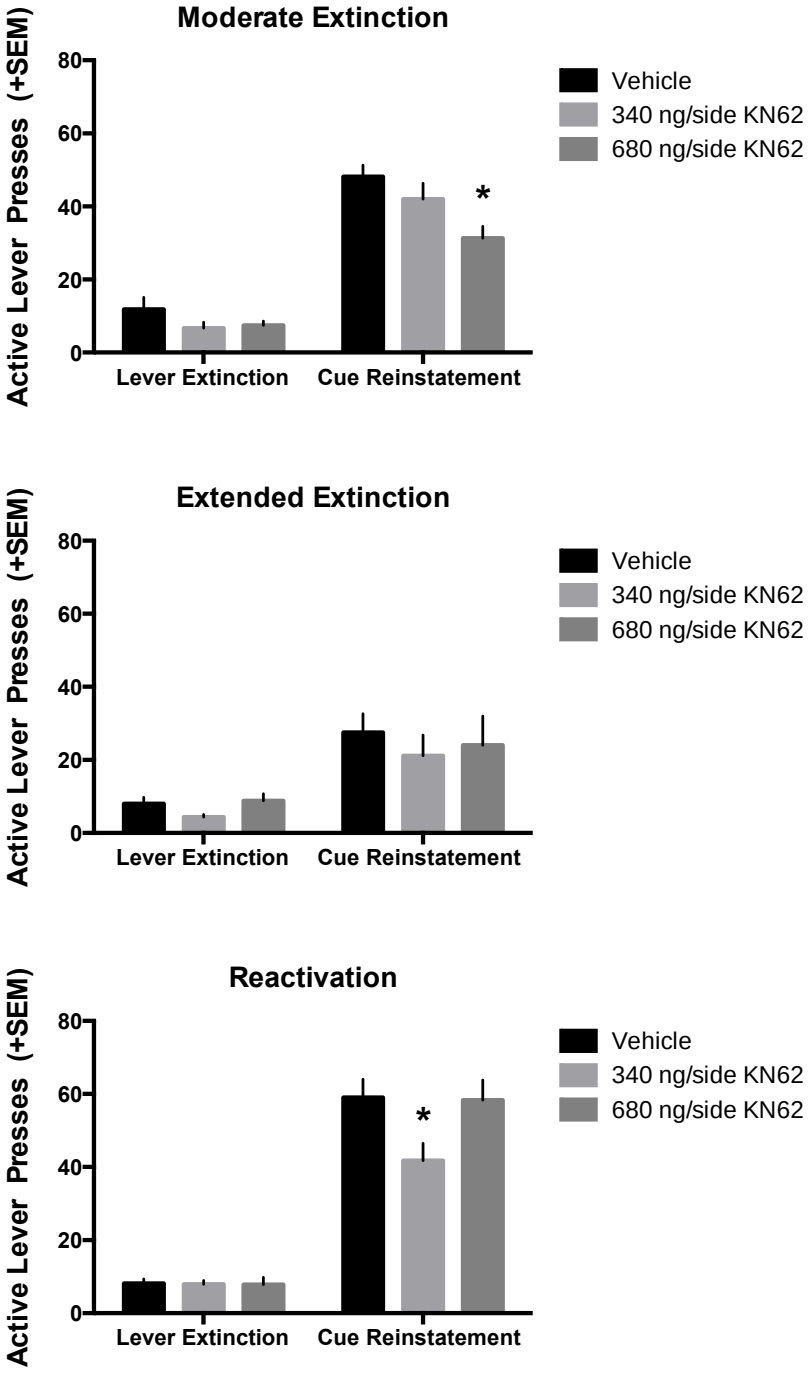

Figure 3. Rats trained to self-administer cocaine paired with an audiovisual cue, underwent either moderate (A) or strong (B) cue exposure (extinction) therapy and then received intra-basolateral amygdala infusion of a vehicle solution or a dose of the CaMKII inhibitor KN62. The next day rats were tested for their propensity to reinstate lever pressing for cocaine relative to baseline responding (relapse). Strong cue exposure reduces reinstatement relative to moderate cue exposure, potentially producing a floor effect. With moderate extinction, KN62 produced a dose-dependent reduction in reinstatement. C) Reactivation of cocaine cue memory followed by low dose KN62 infusion reduced reinstatement. A) Veh: N=6, 340: N=7, 680: N=7 B) Veh: N=8, 340: N=6, 680: N=6 C) Veh: N=11, 340: N=9, 680: N=6.

Research Project 4: Project Title and Purpose

Postoperative Radiation, Cisplatin, and Panitumumab in Head and Neck Cancer – Locally advanced squamous cell carcinoma of the head and neck (SCCHN) is treated with various combinations of radiation and chemotherapy. Epidermal growth factor receptor (EGFR) is highly expressed in SCCHN and its overexpression is associated with poor patient outcome, making EGFR a promising target of anticancer therapy. This Phase II clinical trial seeks to determine whether the addition of an EGFR-specific monoclonal antibody, panitumumab, improves survival of patients with locally advanced SCCHN when combined with the standard of care (radiation plus cisplatin) in the adjuvant setting following surgical resection.

Duration of Project

1/1/2012 – 12/31/2013

Project Overview

Locoregional disease recurrence following surgical resection and adjuvant radiation represents a dominant failure pattern for advanced head and neck cancer patients. Large-scale randomized cooperative group studies have suggested that the addition of cisplatin to radiation in the postoperative setting for high-risk patients may improve overall outcome. The current study is designed to incorporate one of the new molecular EGFR signaling inhibitors (panitumumab) into the postoperative head and neck cancer treatment paradigm in an effort to further improve outcome. The known radiosensitizing effects of cisplatin will also be examined in conjunction with panitumumab in this single-arm Phase II study. Gaining experience regarding the feasibility, toxicity profile, and outcome for patients treated in this Phase II trial will provide a logical platform to consider a future Phase III comparison of this approach against standard postoperative therapy with radiation plus cisplatin.

Forty-seven individuals with locally advanced, newly diagnosed SCCHN will undergo surgical resection with curative intent. Within seven weeks of surgery, patients will be treated with cisplatin chemotherapy in combination with weekly panitumumab and daily external beam radiation. Progression-free survival, overall survival, and treatment toxicities will be determined; EGFR-related and immune biomarkers will be studied in baseline tumor tissue, as well as blood samples obtained before and after therapy. The primary endpoint of the trial is to determine whether the addition of panitumumab to standard adjuvant chemoradiation therapy (CRT) improves survival.

Principal Investigator

Jennifer R. Grandis, MD
Professor of Otolaryngology and of Pharmacology
University of Pittsburgh
200 Lothrop Street
Pittsburgh, PA 15213

Other Participating Researchers

Robert Ferris, MD, PhD – employed by the University of Pittsburgh

Expected Research Outcomes and Benefits

We expect to determine whether the addition of a high immunoglobulin 2- (IgG_2) EGFR monoclonal antibody, in combination with cisplatin and radiation, enhances survival in locally advanced, surgically resected SCCHN when administered in the adjuvant setting. These findings will provide invaluable knowledge as to whether EGFR targeting is useful in the adjuvant setting for SCCHN.

Summary of Research Completed

Forty-seven out of 47 participants (47/47) have been enrolled to date, and the study is now closed to accrual. Patients continue to be followed and a survival analysis is forthcoming; however, preliminary analysis was presented at the 2014 American Society of Clinical Oncology (ASCO) meeting:

Background: Treatment intensification for human papillomavirus (HPV)-negative head and neck cancer (HNC) is an active area of investigation. Targeting the epidermal growth factor receptor (EGFR) pathway using the monoclonal antibody panitumumab (pmAb) with cisplatin (C) chemoradiation was investigated in high-risk resected, primarily HPV-negative HNC patients.

Methods: Eligible were patients with Eastern Cooperative Oncology Group (ECOG) performance status 0-1 with pathologic stage III or IVA squamous cell carcinoma of the oral cavity, larynx, or hypopharynx, without gross residual tumor and with high-risk factors (margins <1mm, extracapsular spread (ECS), perineural/angiolymphatic invasion, or two or more positive lymph nodes). Postoperative treatment started within seven weeks of surgery, consisting of standard radiation therapy (RT) (60-66 Gy, once daily fractions in six to seven weeks) concurrent with weekly pmAb 2.5 mg/kg intravenously (IV) and weekly C 30 mg/m^2 IV. Carboplatin (AUC 1.5 weekly) substitution was allowed for certain C-associated toxicities. The primary endpoint was progression-free survival (PFS).

Results: Of 46 patients accrued, two did not receive pmAb, leaving 44 for analysis. Median age was 58 (range 23-81); 16 percent were female. Primary sites included: oral cavity (73 percent), larynx (20 percent), hypopharynx (5 percent), and oropharynx (2 percent); 86 percent were stage IVA. Indications for adjuvant therapy included ECS (n=23), perineural invasion (n=22), and/or positive margins (n=3). The median follow-up for 32 pts without recurrence was 27 months (range three-67). The two-year PFS was 73 percent (95 percent CI, 61-88 percent) (Figure 1) and the two-year overall survival (OS) was 76 percent (95 percent CI, 64-91 percent) (Figure 2). Twelve patients developed recurrence; eight of them died. An additional five died from other causes. Grade 3/4 toxicities included mucositis (41 percent), hyponatremia (25 percent), leukopenia (25 percent), dysphagia (18 percent), neutropenia (21 percent), nausea/vomiting (14 percent), anorexia (11 percent), rash (9 percent), and neutropenic fever (9 percent). Prophylactic gastrostomy tubes were placed in 43 percent of patients; 18 percent required tube placement

during or after therapy.

Conclusions: Preliminary analysis of adjuvant treatment intensification by adding pmAb to C chemoradiation suggests promising clinical outcome for high-risk, predominantly HPV-negative HNC patients.

Figure 1.

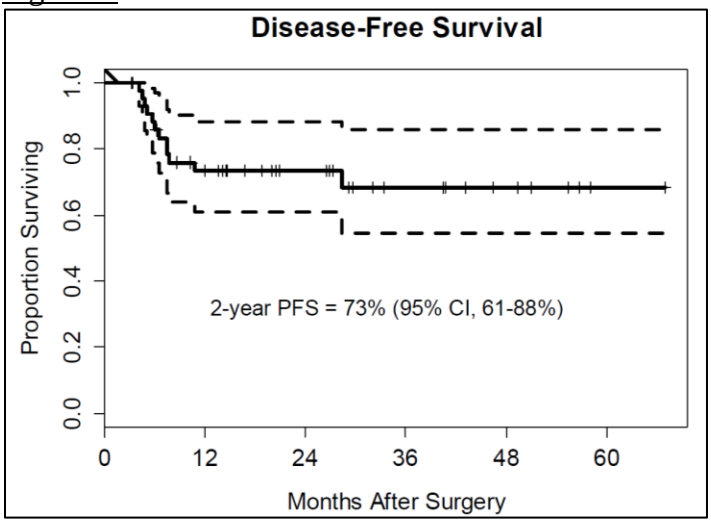

Figure 2.

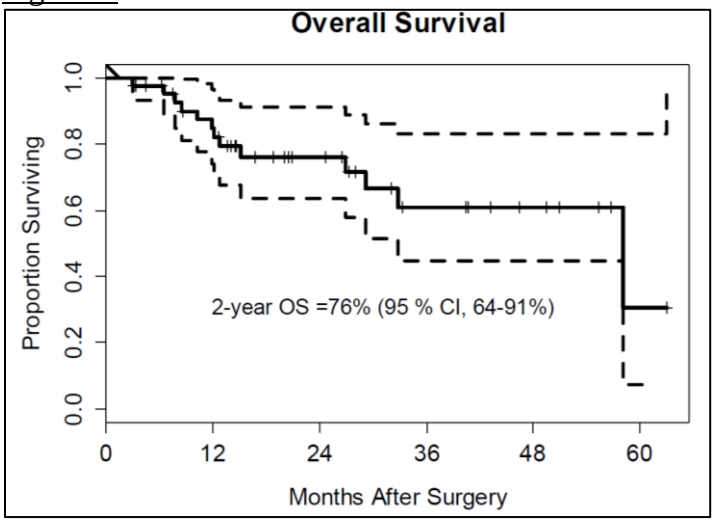

Research Project 5: Project Title and Purpose

Radiation, Cetuximab, and Pemetrexed with/without Bevacizumab in Head and Neck Cancer – Patients with squamous cell carcinoma of the head and neck (SCCHN) are increasingly treated with primary chemoradiotherapy (CRT). The incorporation of novel targeted therapies to CRT is

of major interest since it may potentially improve efficacy without significantly increasing toxicity. This project will test the antitumor efficacy of radiation, cetuximab (a chimeric anti-epidermal growth factor receptor [EGFR] monoclonal antibody [mAb]), and pemetrexed (an anti-folate), with or without bevacizumab (an anti-vascular endothelial growth factor [VEGF] antibody), in patients with locally advanced SCCHN.

Duration of Project

1/1/2012 – 12/31/2013

Project Overview

Patients with head and neck cancer are increasingly treated with nonsurgical therapies. Concurrent administration of radiation and chemotherapy is the preferred way to combine the two modalities. The incorporation of novel targeted therapies to chemoradiotherapy is of particular interest in head and neck cancer and may improve efficacy without significantly increasing toxicity. Cetuximab is an EGFR inhibitor that is a potent radiosensitizer and has increased the survival of patients with stage III/IV head and neck cancer when added to radiation therapy. Pemetrexed is a multi-targeted anti-folate that has demonstrated single agent activity in recurrent or metastatic head and neck cancer. Bevacizumab is a novel agent that targets VEGF and has produced promising results in multiple solid tumors. We hypothesize that the addition of bevacizumab to the combination of cetuximab, pemetrexed, and radiation will result in survival benefit in patients with locoregionally advanced SCCHN. Therefore, we propose a Phase II randomized comparison of cetuximab, pemetrexed, and radiation, with or without bevacizumab.

Eighty patients with locally advanced SCCHN will be enrolled to this study, which will evaluate the progression-free survival (PFS) at two years, locoregional and distant disease-free survival, overall survival, toxicities, and quality of life with the combination of radiation, cetuximab, and pemetrexed, with or without bevacizumab. Also, tumor tissue and baseline blood specimens will be collected from prior diagnostic procedures for future correlative studies.

Principal Investigator

Jennifer R. Grandis, MD
Professor of Otolaryngology and of Pharmacology
University of Pittsburgh
200 Lothrop Street
Pittsburgh, PA 15213

Other Participating Researchers

Julia Bauman, MD, MPH – employed by the University of Pittsburgh

Expected Research Outcomes and Benefits

The major achievement of this project will be the determination of the role of bevacizumab in the

primary treatment of locally advanced, curable SCCHN. Such a study is likely to pave the way for the definitive Phase III trial of this agent in SCCHN.

Summary of Research Completed

As previously reported, this study completed accrual in May 2013, and preliminary results were presented at the head and neck general poster session at the 2013 American Society for Clinical Oncology (ASCO) meeting. During the current reporting period, the final patient completed treatment and trial data have been maturing. Once median follow-up was greater than two years, the clinical data for the primary endpoint—progression-free survival—have been collated, cleaned, and organized into a final database. These data are currently being analyzed by the project biostatistician. No outcomes data from this analysis are currently available; however, they are expected by fall 2014. In addition, we have been evaluating biomarkers associated with angiogenesis and inflammation in archived tumor tissue and serum in patients treated on this trial; the biomarker database is also being correlated with survival outcomes in the context of the primary analysis. Final toxicity data are now being summated, and quality-of-life data are collated and under analysis. A manuscript will be submitted to a high-impact, peer-reviewed oncology journal by the end of 2014.

Research Project 6: Project Title and Purpose

Comparison of Biomarker Modulation in Head and Neck and Lung Cancers – This project will examine the pharmacodynamics of erlotinib versus dasatinib, or a combination of erlotinib plus dasatinib versus placebo, in a presurgical setting of head and neck and lung cancers. This four-arm randomized clinical trial will determine whether biomarkers are modulated by epidermal growth factor receptor (EGFR) and/or Src kinase targeting and whether biomarker modulation is associated with reduction of tumor volume and/or evidence of histologic response in the tumor; the project will also evaluate the safety and tolerability of the treatment regimens. The long-term goal is to determine which patients are most likely to respond to treatment with EGFR inhibitors, Src inhibitors, or a combination of the two.

Duration of Project

1/1/2012 – 12/31/2013

Project Overview

This project consists of a double-blind, placebo controlled, presurgical window of opportunity study that tests the effects of an EGFR tyrosine kinase inhibitor (erlotinib), an Src family kinase inhibitor (dasatinib), or a combination of erlotinib plus dasatinib versus placebo in squamous cell carcinoma of the head and neck (SCCHN) and non-small cell lung cancer (NSCLC) patients undergoing surgical resection of their disease. In addition to acquiring paired blood and tissue samples to identify markers of drug effect, patients will undergo a baseline computed tomography (CT) scan and a CT scan on the day of surgery to determine antitumor effects of the therapy. Specific aims are to: (1) determine the modulation of biomarkers by EGFR and/or Src targeting in head and neck and lung cancers; and (2) determine whether biomarker modulation is

associated with reduction of tumor volume and/or evidence of histologic response in the tumor (e.g., decreased proliferation and/or decreased apoptosis), as well as to evaluate the safety and tolerability of the treatment regimens. The long-term goal of this trial is to determine which SCCHN and NSCLC patients are most likely to respond to treatment with EGFR inhibitors, Src inhibitors, or a combination of the two.

Principal Investigator

Jennifer R. Grandis, MD
Professor of Otolaryngology and of Pharmacology
University of Pittsburgh
200 Lothrop Street
Pittsburgh, PA 15213

Other Participating Researchers

None

Expected Research Outcomes and Benefits

The primary goal of this project is to elucidate the pharmacodynamic properties of EGFR and/or Src inhibitors in SCCHN and NSCLC tumors. These findings will facilitate the rationale for implementation of targeted therapies in those patients most likely to benefit from specific inhibitors.

Summary of Research Completed

Results from this trial were presented at the 2014 American Society of Clinical Oncology (ASCO) meeting:

Background: The epidermal growth factor receptor (EGFR) and Src family kinases are upregulated in squamous cell carcinoma of the head and neck (SCCHN). EGFR interacts with cSrc to activate oncogenic signal transducer and activator of transcription 3 (STAT3) signaling; dual targeting is synergistic in SCCHN cell lines. In preclinical models, phosphorylated cSrc (pSrc) mediates resistance to erlotinib (E), a small-molecule EGFR inhibitor. Baseline over-expression of pSrc was associated with E resistance in our prior window trial. Here, we conducted a four-arm phase 0 trial of E; dasatinib (D), an ATP-competitive inhibitor of cSrc; E+D; versus placebo (P).

Methods: Patients with operable Stage II-IVA SCCHN were randomized 1:1:1:1 to seven-21 days of neoadjuvant E 150 mg daily (n=11), D 100 mg daily (n=13), E+D (n=15), or P (for E; n=14). Paired tumor specimens were collected pre- and post-treatment. The primary endpoint, percent change in response evaluation criteria in solid tumors (RECIST)-measurable index lesions, was compared among groups by two-way analysis of variance (ANOVA). We analyzed the relationship between tumor percent change and pharmacodynamic expression of EGFR and cSrc pathway constituents. Pre-defined, hypothesis-driven analytes included pSTAT3, pSrc,

pMet, and pMAPK.

Results: 58 patients gave consent, 55 were randomized, and 53 were treated. Rash was observed on E arms; gastrointestinal (GI) toxicities were observed in all active treatment groups. There was a significant decrease in tumor size in the E arms (p=0.0014), and no additive or independent effect from D (p=0.24) (Figure 1). Among E-treated patients, high baseline pMAPK expression was associated with reduction in tumor size (p=0.03) (Figure 2). An E-treated patient experiencing complete clinical response harbored a somatic MAPK1 E322K mutation (Figure 3). Among D-treated patients, high baseline pSTAT3 was associated with tumor progression (p=0.03) (Figure 4).

Conclusions: Brief neoadjuvant treatment with E significantly decreased tumor size in operable SCCHN, with no independent or added effect from D. Baseline pMAPK expression and genomic MAPK alterations warrant further study as response biomarkers for anti-EGFR therapy. High basal pSTAT3 in SCCHN patients may be independent of cSrc, explain therapeutic resistance, and preclude further development of D in biomarker-unselected cohorts.

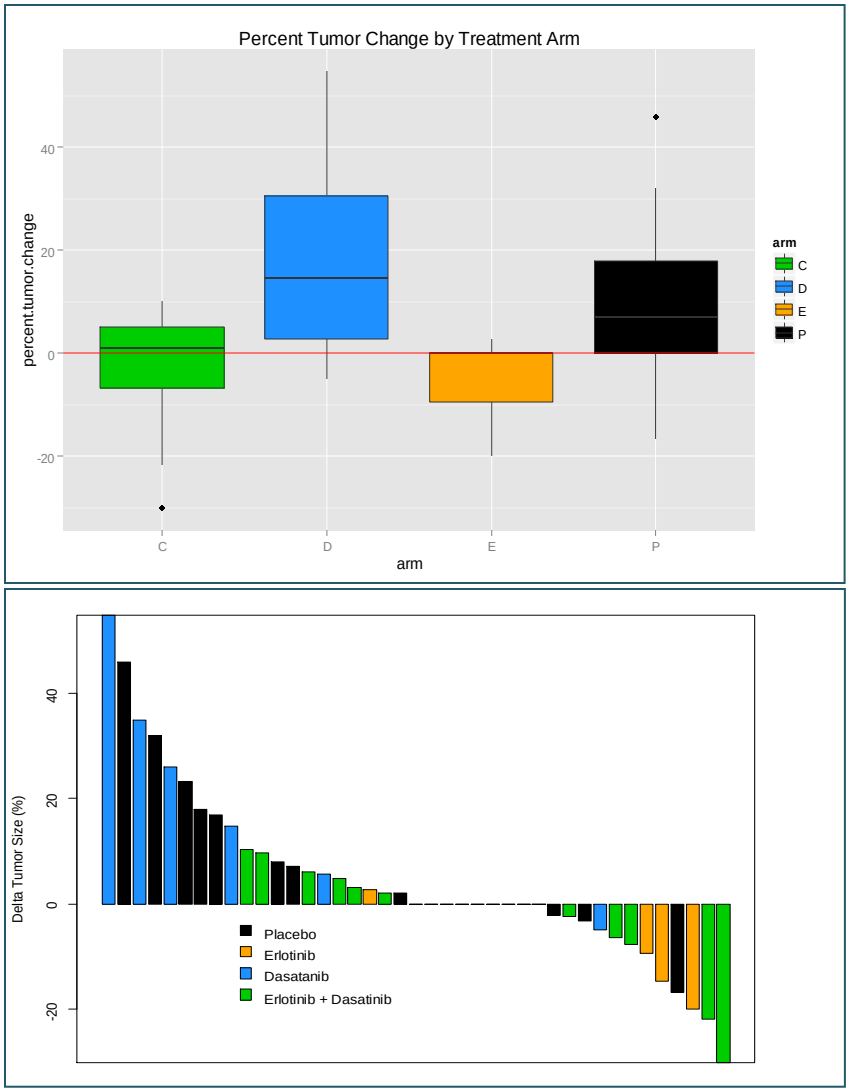

Figure 1. Upper panel: Percent change in RECIST-measurable index lesions was compared among groups by two-way ANOVA. Lower panel: Waterfall plot for individual patient percent tumor response.

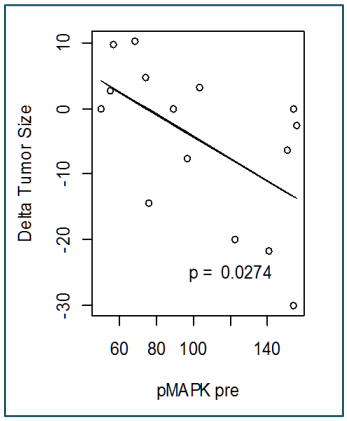

Figure 2. Baseline pMAPK was associated with erlotinib sensitivity (p=0.03).

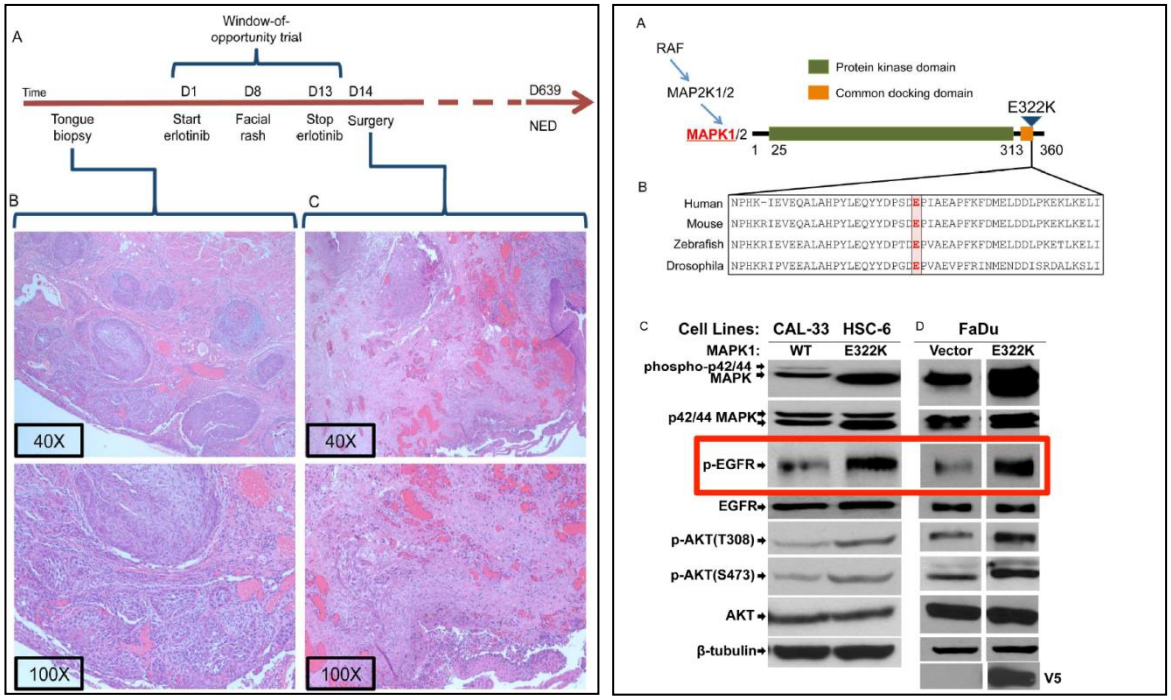

Figure 3. Exceptional responder to erlotinib. Left panel: A patient with clinical T1N2c oral tongue SCC developed a complete clinical response after 14 days of erlotinib. Right panel: Tumor tissue was subjected to next-generation sequencing and found to harbor a *MAPK1 E322K* mutation. Transfection of the mutant *MAPK1* upregulated pEGFR in SCCHN cell lines and conferred erlotinib sensitivity.

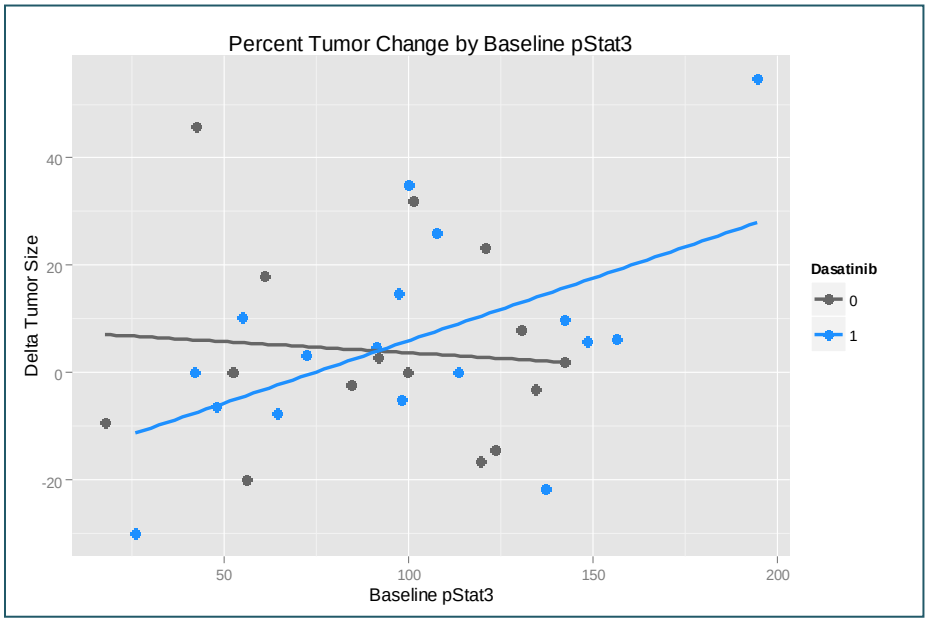

Figure 4. Baseline pSTAT3 was associated with dasatinib resistance (p=0.03).

Research Project 7: Project Title and Purpose

Phase I Study of ABT-888 in Combination with Carboplatin/Paclitaxel in Solid Tumors – Significant advances in cancer treatment have been made over the past 10-15 years. However, when metastatic disease is diagnosed, overall prognosis remains poor. It is clear that new, effective, and less toxic drugs and treatment regimens are needed for our cancer patients. We describe a novel phase I clinical trial that focuses on improving the clinical efficacy of cytotoxic chemotherapy by modulating the process of deoxyribonucleic acid (DNA) repair through inhibition of the key DNA repair enzyme poly(ADP-ribose) polymerase (PARP). We plan to combine the novel PARP inhibitor compound veliparib (ABT-888) with weekly carboplatin and paclitaxel in patients with advanced solid tumors.

Duration of Project

1/1/2012 – 12/31/2013

Project Overview

Increased PARP protein expression and/or enzymatic activity is one mechanism by which human tumor cells are able to avoid the apoptotic effects induced by DNA damaging agents, resulting in the development of cellular drug resistance. PARP activity is essential for the repair of single-strand DNA breaks through the base excision repair (BER) pathway. Thus, inhibition of PARP is able to sensitize tumor cells to cytotoxic agents that induce DNA damage that would normally be repaired through the BER system. In addition, preclinical studies have shown that inhibition of PARP is lethal to cells with an impaired ability to repair double-strand DNA breaks, such as those with BRCA (breast cancer) mutations. This phase I clinical trial is focused on defining the optimal use of veliparib, a novel, small-molecule, orally dosed PARP inhibitor, in combination with cytotoxic chemotherapy in patients with advanced solid tumors.

The primary aim of this phase I dose escalation study is to determine the maximum tolerated dose (MTD) and dose-limiting toxicity (DLT) of veliparib with carboplatin and paclitaxel in patients with advanced cancers. A secondary aim of the trial is to determine the level of PARP inhibition and DNA damage in tumor samples, peripheral blood mononuclear cells (PBMCs), and other normal tissues.

Principal Investigator

Edward Chu, MD
Professor of Medicine and Pharmacology and Chemical Biology
University of Pittsburgh
5150 Centre Avenue
Pittsburgh, PA 15232

Other Participating Researchers

Jan Beumer, PharmD, PhD – employed by the University of Pittsburgh

Expected Research Outcomes and Benefits

The major outcome of this trial will be the determination of an appropriate dose of veliparib to be combined with a chemotherapy regimen that can then be used for a subsequent phase II clinical trial. We also expect to gain a better understanding of the specific side effects associated with the combination of the PARP inhibitor veliparib with carboplatin and paclitaxel. We will also gain additional knowledge regarding the clinical pharmacology of veliparib when it is combined with cytotoxic chemotherapy, as well as the actual biological activity and mechanism of action of veliparib. Although not a primary endpoint of this study, we plan to obtain important information about the potential clinical efficacy of veliparib when combined with carboplatin and paclitaxel.

Summary of Research Completed

As noted in last year's progress report, a supplement from the National Cancer Institute (NCI) to the grant 1U01- CA099168-06 provides support for an additional cohort of participants in this study who carried a deleterious germline mutation in BRCA1 or BRCA2. The rationale for this cohort is exploitation of the known synthetic lethal relationship between BRCA (homologous recombination DNA repair) and PARP (base excision DNA repair, or BER). In patients with deleterious BRCA germline mutations, somatic cells possess one functional copy of the affected BRCA gene, whereas malignant cells will have suffered loss of heterozygosity and phenotypically lack BRCA function. When the study was initiated, it was unknown whether the maximum tolerated dose (MTD) of the PARP inhibitor/carboplatin/paclitaxel combination would be equivalent in wild type and germline mutation carrier individuals. Thus, the primary objective of this portion of the study was to determine the recommended phase II dose of the ABT-888/carboplatin/paclitaxel combination in BRCA mutation carriers.

During the previous reporting period, the recommended phase II dose for patients with advanced solid malignancies (Part A) was found to be: carboplatin AUC=6, paclitaxel 200 mg/m^2, and ABT-888 100 mg bid. It appears that the recommended phase II dose for patients with advanced solid malignancies who have a deleterious germline mutation in the BRCA1 or BRCA2 gene (Part B) is carboplatin AUC=6, paclitaxel 150 mg/m^2, and ABT-888 20 mg bid.

While patient enrollment to Part A was completed during the previous reporting period, enrollment to Part B of this study was completed during the current reporting period. A total of 111 subjects were enrolled. Dose-limiting toxicities in Part A and Part B included thrombocytopenia and neutropenia. The recommended phase II dose in Part B is at a significantly 5-fold lower dose of ABT-888 (20 mg bid) than the recommended phase II dose in Part A (100 mg bid). The recommended dose of paclitaxel was also lower for cohort B. One possible explanation for the lower doses of ABT-888 and paclitaxel is that the combination regimen is more myelosuppressive in individuals who carry a germline BRCA1 or BRCA2 mutation. An alternative explanation is that subjects enrolled in the maximally administered dose level of cohort B were more heavily pretreated than those in Part A, and it is conceivable that this factor may explain the toxicity observed at this dose level in Part B.

With respect to antitumor activity, tumor responses were seen in both Part A and Part B,

including complete responses in three participants with breast cancer and one participant with urothelial cancer.

Our pharmacokinetics (PK) laboratory has been investigating the clinical pharmacology and drug metabolism of the individual drugs used in this study. Carboplatin area under the curve (AUC) was determined by intensive sampling. In Figure 1, the green curve depicts the AUC values determined in patients (ordinally ordered on the X-axis). As observed, the target AUC of 6 is the approximate mean of this distribution, but there is quite a range of measurements around this target value. Patients with AUC less than 6 may well be receiving sub-therapeutic doses, while patients who received more than AUC6 may well have experienced unnecessary toxicities. The red curve in Figure 1 depicts a predicted carboplatin AUC based on a single sample determination, followed by a limited sampling strategy (LSS) estimation according to Ghazal-Aswad. The distribution is very similar to the actually measured AUC. The percent error of the Ghazal-Aswad estimation versus patient number is plotted in Figure 2. On average, this approach is accurate; but in many individuals (38 percent), the estimate is more than 25 percent different from the actually measured AUC.

Also during the project period, pharmacodynamics (PD) biomarker studies investigating poly(ADP-ribose) (PAR) and H2A histone family member X (γ-H2AX) levels were performed; formal analysis is currently underway.

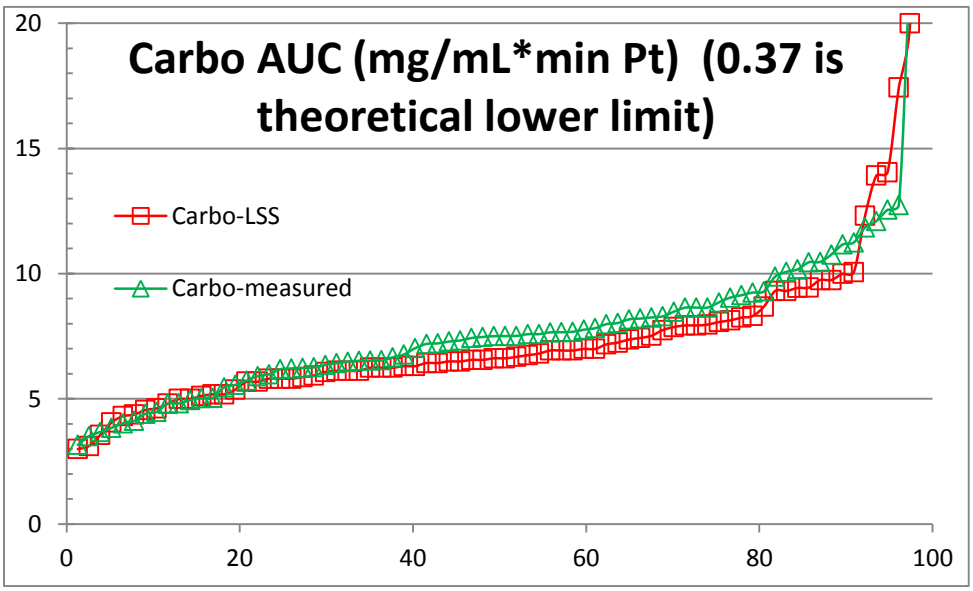

Figure 1. Predicted and actual carboplatin AUC. The red curve depicts a predicted carboplatin AUC based on a single sample determination, followed by a limited sampling strategy (LSS) estimation according to Ghazal-Aswad. The distribution is very similar to the actually measured AUC (green curve).

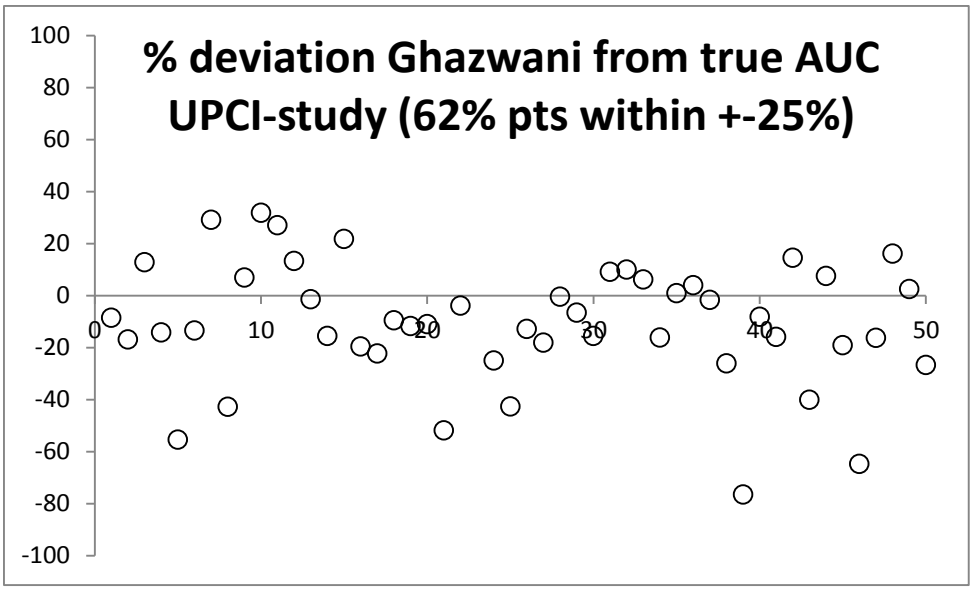

Figure 2. Percent error of the Ghazal-Aswad estimation versus patient number. On average, this approach is accurate; but in many individuals (38 percent), the estimate is more than 25 percent different from the actually measured AUC.

Research Project 8: Project Title and Purpose

Veliparib Therapy in Advanced Biliary, Pancreatic, Urothelial, and Non-Small Cell Lung Cancer– Significant advances in cancer treatment have been made over the past 10-15 years. However, when metastatic disease is diagnosed, overall prognosis remains poor. It is clear that new, effective, and less toxic drugs and treatment regimens are needed. We describe a novel phase I clinical trial that focuses on improving the clinical efficacy of cytotoxic chemotherapy by modulating the process of deoxyribonucleic acid (DNA) repair through inhibition of the key DNA repair enzyme poly(ADP-ribose) polymerase (PARP). We plan to combine the novel PARP inhibitor compound veliparib (ABT-888) with cisplatin plus gemcitabine in patients with advanced biliary, pancreatic, urothelial, and non-small-cell lung cancer (NSCLC).

Duration of Project

1/1/2012 – 12/31/2013

Project Overview

Increased PARP protein expression and/or enzymatic activity is one mechanism by which human tumor cells are able to avoid the apoptotic effects induced by DNA damaging agents, resulting in the development of cellular drug resistance. PARP activity is essential for the repair of single-strand DNA breaks through the base excision repair (BER) pathway. Thus, inhibition of PARP is able to sensitize tumor cells to cytotoxic agents that induce DNA damage that would normally be repaired through the BER system. In addition, preclinical studies have shown that inhibition of PARP is lethal to cells with an impaired ability to repair double-strand DNA breaks, such as

those with BRCA (breast cancer) mutations. This phase I clinical trial is focused on defining the optimal use of veliparib, a novel, small-molecule, orally dosed PARP inhibitor, in combination with cytotoxic chemotherapy in patients with advanced cancers.

The primary aim of this phase I dose escalation study is to determine the maximum tolerated dose (MTD) and dose-limiting toxicity (DLT) of veliparib with cisplatin and gemcitabine in patients with advanced biliary, pancreatic, urothelial, and NSCLC. A secondary aim of the trial is to determine the level of PARP inhibition and DNA damage in tumor samples, peripheral blood mononuclear cells (PBMCs), and other normal tissues.

Principal Investigator

Edward Chu, MD
Professor of Medicine and Pharmacology and Chemical Biology
University of Pittsburgh
5150 Centre Avenue
Pittsburgh, PA 15232

Other Participating Researchers

Jan Beumer, PharmD, PhD – employed by the University of Pittsburgh

Expected Research Outcomes and Benefits

The major outcome will be the determination of an appropriate dose of veliparib to be combined with the chemotherapy regimen, which can then be used for a subsequent phase II clinical trial. We also expect to gain a better understanding of the specific side effects that are associated with the combination of the PARP inhibitor veliparib with cisplatin and gemcitabine. We will also gain additional knowledge regarding the clinical pharmacology of veliparib when it is combined with cisplatin and gemcitabine, as well as the actual biological activity and mechanism of action of veliparib. Although not a primary endpoint of this study, we plan to obtain important information about the potential clinical efficacy of veliparib when combined with cytotoxic chemotherapy.

Summary of Research Completed

For this phase I study, eligible patients had metastatic or unresectable disease and had not received prior chemotherapy. Normal renal, hepatic, and bone marrow function were required. ABT-888 was administered twice daily on days 1-12 of each 21-day cycle. Gemcitabine was administered on day 3 and day 10 over 30 minutes, and cisplatin was administered on day 3. The schedule of study treatments is shown in Figure 1. The planned dose levels followed a modified Fibonacci scheme, starting at dose level 1: gemcitabine 750 mg/m^2, cisplatin 75 mg/m^2, and ABT-888 10 mg PO bid (Table 1).

As previously reported, eight participants were enrolled in this phase I study (Table 2). Three were enrolled in dose level 1 with no dose-limiting toxicities (DLT), and five were enrolled in

dose level 2 with one DLT (nausea and vomiting). Myelosuppression was seen in a number of participants, frequently requiring dose reduction.

Unfortunately, the maximum tolerated dose (MTD) could not be determined as specified by the protocol, given the early termination of the study by the sponsor (National Cancer Institute Cancer Therapy Evaluation Program, NCI/CTEP). However, as noted above, myelosuppression was observed in cycle 1 and beyond the degree that is normally observed with the gemcitabine/cisplatin combination regimen at the doses used in this study. This finding suggests a clear enhancement of the cytotoxic effect of the gemcitabine/cisplatin regimen with the addition of veliparib. Based on the degree of myelosuppression observed in this study, there is no recommended phase II dose for this combination. A manuscript describing the results of this study is in preparation, and plans are in place to submit this manuscript to the peer-reviewed journal *The Oncologist*.

The gemcitabine [Y(1)] and metabolite dFdU [Y(2)] data from this clinical trial have been combined with the data from another gemcitabine trial to develop a population pharmacokinetic (POP-PK) model. The performance of this model is adequate, as the predicted and observed data are concordant (Figure 2). This model will be used to develop a limited sampling strategy (LSS) to allow facile determination of essential pharmacokinetic parameters, like clearance, with a minimum of blood draws required.

Figure 1. Treatment schedule.

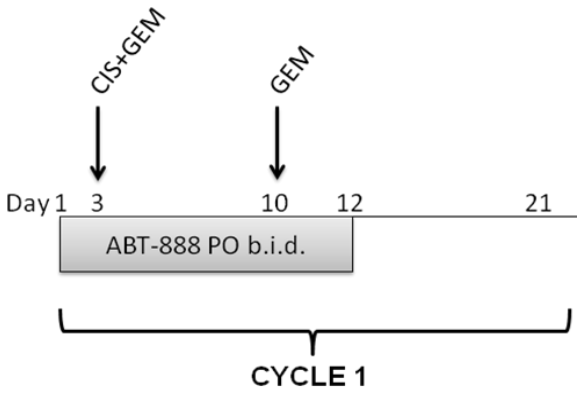

Table 1. Dosing scheme.

DOSE LEVEL	GEMCITABINE	CISPLATIN	Veliparib (ABT-888)
-1	600 mg/m2	75 mg/m^2	10 mg bid
1*	750 mg/m^2	75 mg/m^2	10 mg bid
2	750 mg/m^2	75 mg/m^2	20 mg bid
3	1000 mg/m^2	75 mg/m^2	20 mg bid
4	1000 mg/m^2	75 mg/m^2	50 mg bid
5	1000 mg/m^2	75 mg/m^2	80 mg bid
6	1000 mg/m^2	75 mg/m^2	120 mg bid
7	1000 mg/m^2	75 mg/m^2	200 mg bid

Table 2. Participant notes.

Subject ID	Dose Level	Evaluable	DLT	Subject Notes
01-01-01	1	Yes	No	Removed after 6 cycles for progressive disease
01-01-02	1	Yes	No	Removed after 5 cycles for progressive disease
01-01-03	1	Yes	No	Removed after 2 cycles for progressive disease
02-02-04	2	Yes	No	Removed after 1 cycle for non-compliance
01-02-05	2	Yes	Yes	Removed in cycle 2 for low platelets; gem could not be further dose-reduced
03-02-06	2	Yes	No	Removed after 5 cycles for clinical progression
02-02-07	2	Yes	No	Removed after 4 cycles for progressive disease
01-02-08	2	Yes	No	Removed in cycle 3 due to myelosuppression.

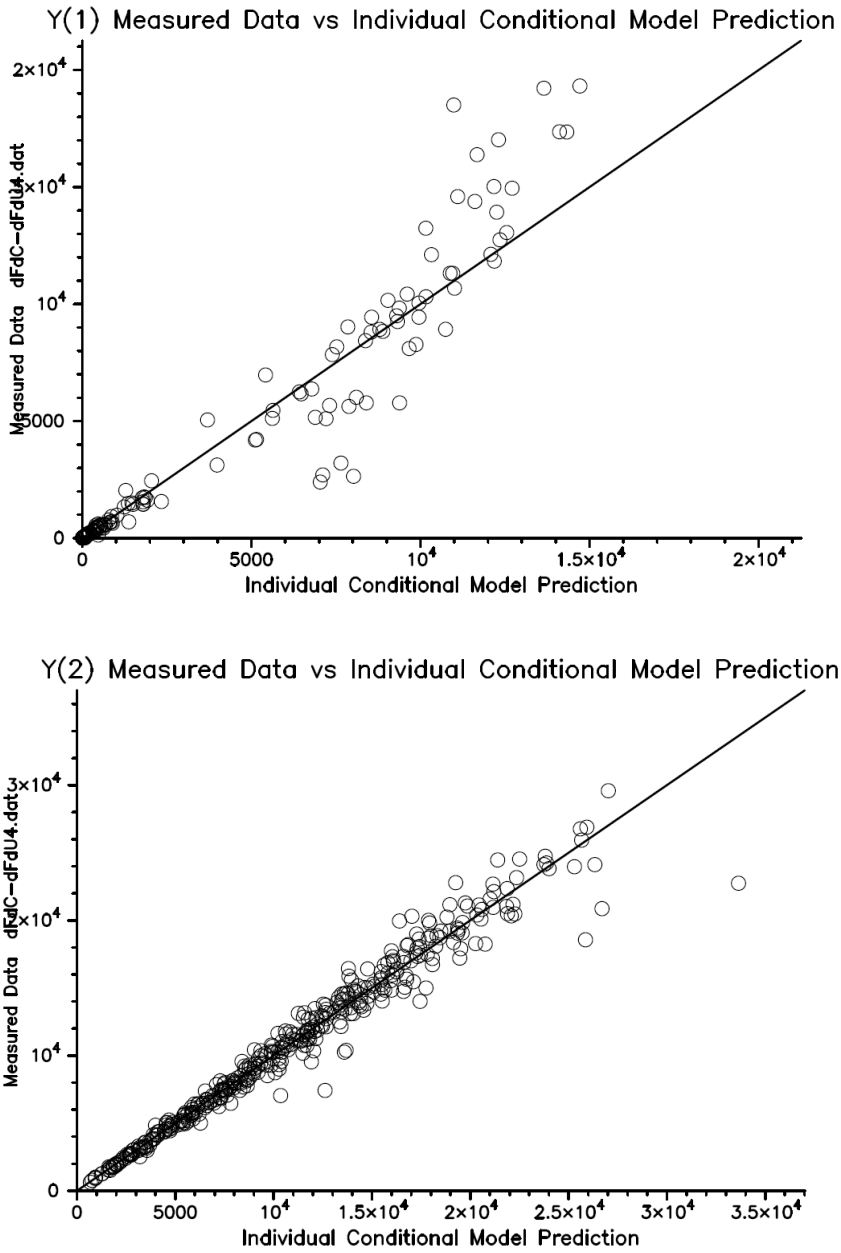

Figure 2. Gemcitabine [Y(1)], top, and metabolite dFdU [Y(2)], bottom, measured values plotted against predicted values.

Research Project 9: Project Title and Purpose

Early Phase I Study of ABT-888 in Patients with Hepatic/Renal Dysfunction and Solid Tumors– Significant advances in cancer treatment have been made over the past 10-15 years. However, when metastatic disease is diagnosed, overall prognosis remains poor. It is clear that new, effective, and less toxic drugs and treatment regimens are needed for our cancer patients. In this project, we will conduct a novel phase I clinical trial that focuses on improving the clinical

efficacy of cytotoxic chemotherapy by modulating the process of deoxyribonucleic acid (DNA) repair through inhibition of the key DNA repair enzyme poly(ADP-ribose) polymerase (PARP). We plan to combine the novel PARP inhibitor compound veliparib (ABT-888) with carboplatin and paclitaxel in patients with solid tumors who have underlying liver or kidney dysfunction.

Duration of Project

1/1/2012 – 12/31/2013

Project Overview

This phase I clinical trial is focused on defining the optimal use of veliparib, a novel small-molecule, orally dosed PARP inhibitor, in combination with cytotoxic chemotherapy in patients with hepatic or renal dysfunction and solid tumors.

The primary aim of this phase I dose-escalation study of veliparib combined with carboplatin and paclitaxel is to determine the maximum tolerated dose (MTD) of veliparib in patients with advanced cancers who suffer from liver and/or kidney dysfunction. This is a unique study performed only once in the early development of a drug and will define how patients with organ dysfunction should be treated with veliparib.

Principal Investigator

Edward Chu, MD
Professor of Medicine and Pharmacology and Chemical Biology
University of Pittsburgh
5150 Centre Avenue
Pittsburgh, PA 15232

Other Participating Researchers

Jan Beumer, PhD – employed by the University of Pittsburgh

Expected Research Outcomes and Benefits

We expect to gain an enhanced understanding of the side effects observed when veliparib is combined with cytotoxic chemotherapy in the setting of liver or kidney dysfunction. Moreover, we plan to gain improved understanding of the clinical pharmacology and metabolism of veliparib in patients with varying degrees of liver or kidney dysfunction. Although clinical efficacy is not a primary endpoint of this organ dysfunction study, we hope to gain some insights into the clinical activity of the combination of veliparib plus carboplatin and paclitaxel in this particular patient population.

Summary of Research Completed

This is a multicenter study that is being coordinated by the University of Pittsburgh Cancer

Institute, and our phase I team has been working with 12 other cancer centers, including Penn State/Hershey Cancer Center, Cancer Institute of New Jersey, Emory Winship Cancer Center, University of California Davis, City of Hope Cancer Center, Memorial Sloan-Kettering Cancer Center, University of Wisconsin, Johns Hopkins Kimmel Cancer Center, Case Western Seidman Cancer Center, Albert Einstein Cancer Center, Wayne State Karmanos Cancer Center, and Dana-Farber Cancer Institute.

To date, 65 patients have been enrolled. As part of this phase I study, there is a normal cohort (patients have normal renal and hepatic function), three renal dysfunction cohorts (moderate, severe, and very severe), and three hepatic dysfunction cohorts (mild, moderate, and severe). As of June 30, 2014, 17 patients have been enrolled on the normal cohort, 28 patients have been enrolled to the renal dysfunction cohort, and 19 patients have been enrolled to the hepatic dysfunction cohort.

Enrollment to the normal cohort is complete. Enrollment to the moderately severe and severe hepatic dysfunction cohorts has been closed because of dose-limiting toxicities secondary to myelosuppression. Enrollment to the R2 moderate renal dysfunction cohort was recently closed because of dose-limiting toxicity secondary to myelosuppression. At present, the only remaining cohort that is actively enrolling participants is the R3 severe renal dysfunction group.

With respect to antitumor activity, tumor responses have been observed in two patients with metastatic breast cancer and one patient with urothelial cancer.

Our pharmacokinetics (PK) laboratory has been investigating the clinical pharmacology and drug metabolism of the individual drugs used in this organ dysfunction study. As reported previously, ABT-888 did not significantly affect the metabolism and PK of carboplatin or paclitaxel. The metabolism of ABT-888 was not altered in the hepatic dysfunction cohort. In contrast, in the renal dysfunction cohort, a significant increase was observed in C_{max} and AUC levels of both parent ABT-888 and the ABT-888 metabolite M8.

The preliminary results of this phase I study were recently presented at the 2014 annual meeting of the American Society of Clinical Oncology (Abstract #2572), and the following conclusions were made:

- ABT-888 combined with carboplatin and paclitaxel is not safely deliverable in patients with moderate to severe hepatic dysfunction as a result of dose-limiting myelosuppression.
- The clinical pharmacology of ABT-888 is unaffected by hepatic dysfunction.
- Renal dysfunction resulted in increased ABT-888 and M8 drug metabolite exposure.
- These data will guide potential dose reductions in patients with hepatic or renal dysfunction.
- PK analysis of carboplatin and paclitaxel in this population is ongoing.

Research Project 10: Project Title and Purpose

Proteomics Analysis of Human Lung Disease – We will use state-of-the-art mass spectrometry (MS) and multiplexed immunoassay platforms and workflows to discover and validate candidate lung disease biomarkers in lung tissue and plasma/serum and to develop biomarker panels and predictive models of nonmalignant chronic lung disease (CLD) and malignant lung disease. These models will find potential clinical application in early detection and diagnosis of disease and prediction of disease progress and patient survival in patients with chronic obstructive pulmonary disease (COPD), emphysema, idiopathic pulmonary fibrosis (IPF), and non-small cell lung cancer (NSCLC).

Duration of Project

1/1/2012 –6/30/2013

Summary of Research Progress

This project ended during a prior state fiscal year. For additional information, please refer to the Commonwealth Universal Research Enhancement Annual C.U.R.E. Reports on the Department's Tobacco Settlement/Act77 Web page at http://www.health.state.pa.us/cure.

Research Project 11: Project Title and Purpose

Mechanisms of Myeloma Cell Regulation of Gfi1 Function in BMSC – Osteolytic lesions in multiple myeloma (MM) rarely heal, even when patients are in long-term remission, due to the persistent MM-induced suppression of bone marrow stromal cell (BMSC) differentiation into bone-forming osteoblasts (OB). We have shown that MM cells induce the expression and function of the transcriptional repressor growth factor independence 1 (Gfi1) in BMSC, which binds to and represses the key transcription factor, Runx2, driving OB differentiation. In this study, we will investigate the mechanisms by which MM cells elevate Gfi1 and induce its nuclear translocation, and its repression of Runx2. This information may lead to the development of bone tissue targeted therapies that block Gfi1 and recover bone formation.

Anticipated Duration of Project

7/19/2013 – 6/30/2015

Project Overview

Osteolytic lesions in multiple myeloma (MM) rarely heal, even when patients are in long-term remission due to persistent MM-induced suppression of bone marrow stromal cell (BMSC) differentiation into functional bone-forming osteoblasts (OB). The continued inability of BMSC to differentiate into OB, even in the absence of MM cells, suggests that MM cells induce a persistent change in BMSCs. Analysis of MM-exposed BMSC revealed that OB suppression results from repression of the critical OB transcription factor Runx2. This repression is due to elevated expression of the transcriptional repressor, growth factor independence 1 (Gfi1), which

can mediate epigenetic changes through chromatin remodeling by recruiting histone-modifying enzymes. Analyses revealed that MM cells induce Gfi1 to bind to a specific site in the Runx2 promoter that is required for Runx2 repression. Of particular interest, MM cells also induce nuclear localization of Gfi1 in MC4 cells, whereas under basal conditions, Gfi1 is predominantly cytoplasmic. Further, we found that BMSC from *Gfi1*$^{-/-}$ mice are significantly resistant to *ex vivo* MM-induced suppression of Runx2. Importantly, *Gfi1* knockdown in BMSC from 2 (of 2) MM patients or MM-pre-exposed MC4 cells significantly restored expression of *Runx2* as well as the OB differentiation markers *Ocn* and *Bsp*. <u>These data indicate that MM cells increase *Gfi1* expression, which in turn represses *Runx2* expression and OB differentiation.</u> Therefore, we believe that targeting Gfi1 expression will reverse OB suppression and, thereby, decrease environmental support of MM cells, leading to decreased tumor burden and bone lysis. To determine the most appropriate way to target Gfi1 function in BMSC, it is necessary to determine the mechanisms involved in MM induction of Gfi1, regulation of localization, and repression of *Runx2*, which are currently unknown. We will use a host of molecular biology techniques to pursue the following aims: 1) determine the mechanisms by which MM cells upregulate Gfi1 expression in BMSC; and 2) determine the mechanisms by which MM cells induce Gfi1 nuclear translocation and activate Gfi1 repression of *Runx2* in BMSC, by investigating the role of Gfi1 protein modifications in the generation of the MM-altered BMSC phenotype.

Principal Investigator

Deborah L. Galson, PhD
Research Assistant Professor
Hillman Cancer Center Res Pav Rm 1.19b
5117 Centre Avenue
Pittsburgh, PA 15213

Other Participating Researchers

Quanhong Sun, PhD; Juraj Adamik, PhD – employed by University of Pittsburgh

Expected Research Outcomes and Benefits

Multiple myeloma (MM) is the most frequent cancer to involve the skeleton, with up to 90% of patients developing bone lesions that can result in severe bone pain and frequent pathological fractures. Unfortunately, these lytic bone lesions rarely heal due to the permanent MM alteration of osteoblast (OB) precursors that prevents differentiation into functional bone-forming OB and enhances support of MM. This project will investigate the mechanisms by which MM cells alter the behavior of the OB precursors. We have identified a transcriptional repressor, Gfi1, that plays a key role in repressing Runx2 expression, a transcription factor absolutely required for OB differentiation and bone formation. The expected outcome is that we will gain information about the signal pathways and transcription factors that MM cells activate to elevate Gfi1 expression in bone marrow stromal cells (BMSC). In addition, we will develop an understanding of the protein modifications induced by MM cells to regulate Gfi1 nuclear translocation and repression of the *Runx2* gene in BMSC, thereby suppressing OB differentiation. Further, we will acquire insight

into the chromatin alterations brought about on the *Runx2* gene that maintain repression in MM bone disease. Gfi1 has important roles in other cells in the body but undergoes a lot of tissue-specific regulation. The information on Gfi1 regulation in BMSC will aid in the determination of useful targets for selective inhibition of Gfi1, which could result in restoration of OB differentiation without damaging other cells/tissues in the body.

Summary of Research Completed

Aim 1: Determine the mechanisms by which MM cells upregulate Gfi1 expression in BMSC. *Our initial hypothesis is that MM cell activation of the CCAAT-enhancer-binding protein (C/EBP) family is the most likely mechanism of increasing Gfi1 expression, but X-box binding protein 1s (Xbp1s) may act directly on the Gfi1 gene as well via an enhancer.*

Multiple myeloma (MM) cells alter bone marrow stromal cells (BMSC) so that they have a decreased capacity to respond to osteoblast differentiation signals via Gfi1 repression of Runx2 expression. We reported in our preliminary results that human BMSC from MM patients exhibit increased expression of an endoplasmic reticulum (ER) stress indicator protein GRP78/BIP when compared to BMSC from healthy donors. *In vitro* co-culture of MM cells with the murine pre-osteoblast cell line MC4 increased expression of both Gfi1 mRNA and several ER stress responder genes reflecting activation of the cellular response cascades, termed the unfolded protein response (UPR), that are initiated by the ER-resident transmembrane sensors protein kinase RNA-like ER kinase (PERK), inositol-requiring enzyme 1α (Ire1α, ERN1), and activating transcription factor 6 (ATF6). The classic ER stress inducers tunicamycin (TM) and thapsigargin (TG) both increase Gfi1 mRNA in the pre-osteoblast murine cell line MC4. We used TG treatment of MC4 cells in the presence and absence of the inhibitor actinomycin D to demonstrate that TG increased Gfi1 mRNA via increased transcription in the pre-osteoblast cell line MC4 (Figure 1). To confirm that MM cell exposure (48 hours) and TG treatment (6 hours) increased Gfi1 transcription, we used chromatin immunoprecipitation (ChIP) to evaluate the level of histone modifications, acetylated histone H3 at position K9 (H3K9ac) and trimethylated H3 at position K4 (H3K4me3), that reflect the transcriptional activity of a promoter region (Figure 2). We found that MM cell exposure and TG increased both H3K9ac and H3K4me3 at mouse mGfi1 promoters P1 and P2, indicating increased transcription. In contrast to the Gfi1 gene, our studies of the *Runx2* gene revealed that MM exposure induced both H3K9ac and H3K4me3 to go down at the *Runx2* P1 promoter (not shown). Currently, the Gfi1 P1 and P2 exon-1-specific quantitative real-time polymerase chain reaction (qRT-PCR) analysis of promoter usage has been challenging since the RT step has to be very efficient and get through the 5'end of the mRNA. However, the strength of the changes of the histone marks was stronger at Gfi1 P1 than at P2 (Figure 2), suggesting that P1 is more activated by MM cell exposure than P2 in MC4 cells.

In our preliminary results, we had shown that the ER stress sensor Ire1α is activated in MC4 cells by MM cell exposure, leading to the generation of the transcription factor Xbp1s via the Ire1α endoribonuclease (RNase) activity. Inhibition of the Ire1α RNase activity by SML0149 completely abrogated TG induced Ire1α production of Xbp1s and induction of Gfi1 mRNA (Figure 3). Ire1α also has a JNK (c-Jun N-terminal kinase) activity; we have refined our

preliminary data to show that pretreatment with JNK inhibitor SP600126 did not affect the PERK pathway activation of eIF2α but completely blocked TG-induced c-Jun phosphorylation (Figure 3). Although SP600126 blocked JNK activity completely, it only partially blocked the Gfi1 mRNA increase. These data indicate that Ire1α-mediated JNK activation only partially induced Gfi1 upregulation, whereas the Ire1α RNase activity appears to be required for TG-induced Gfi1 upregulation. To clarify the roles of Ire1α RNase and kinase activities in the induction of Gfi1 expression, we over-expressed wild-type and mutant human Ire1α in MC4 cells (Figure 4). Over-expression of wild-type or kinase-deficient (K599A) Ire1α in MC4 cells in the absence of ER stressor treatment increased the expression of Gfi1 mRNA. However, over-expression of RNase-deficient (K907A) Ire1α had no effect on Gfi1 expression. This observation recapitulates the finding from the inhibitor studies in Figure 3. We previously reported that tumor necrosis factor alpha (TNFα) and interleukin 7 (IL-7) produced by MM cells played a large role in *Runx2* repression and could induce Gfi1. The Ire1α RNase inhibitor SML0149 also blocked TNFα repression of *Runx2* in MC4 cells and in human BMSC (Figure 5). Ire1α knockdown (not shown) decreased Gfi1 upregulation by MM and prevented MM cell induced *Runx2* repression (Figure 6).

We have begun studies looking for MM induced C/EBP, NF-κB, STAT1/3, and Xbp1s binding to the *Gfi1* gene, but we have had technical difficulties that have slowed our progress. However, these are now largely resolved. We have preliminary data that MM cells increase C/EBPβ occupancy on the *Gfi1* gene at several positions within the -1000/+1 P1 region (not shown). We are also in the midst of inhibitor studies to delineate which signaling pathways are important for MM cells to activate the *Gfi1* gene in MC4 cells. IL-7 induction of Gfi1 is not blocked by NFκB activation inhibitor-III or a MEK inhibitor U0126. However, it is blocked by the JAK/STAT inhibitor WP1066 and the PI3K inhibitor LY294002 (not shown).

<u>Aim 2</u>: Determine the mechanisms by which MM cells induce Gfi1 nuclear translocation and activate Gfi1 repression of *Runx2* in BMSC by investigating the role of Gfi1 protein modifications in the generation of the MM-altered BMSC phenotype. *Our hypothesis is that acetylation and phosphorylation are negative regulators of Gfi1 and SUMOylation increases Gfi1 repressor activity.*

We had reported in the preliminary results that we detected acetylation of Gfi1 protein in the presence of a combination of deacetylase inhibitors, trichostatin-A (TSA) and nicotinamid (NAM), and that mutation of a putative acetylation site K292R in zinc finger 2 completely blocked Gfi1 acetylation. We have conducted studies to determine the function of acetylation at K292. Gfi1 binding site biotin-oligo pulldown of HEK293 cell extracts programmed by transfection with either Gfi1-WT or Gfi1-K292R revealed that the K292R mutation increased the binding capacity of Gfi1, indicating that Gfi1 acetylation decreases DNA binding (Figure 7). Further, co-transfection studies demonstrated that the Gfi1-K292R was a stronger *Runx2*-Luc repressor than Gfi1-WT and is insensitive to inhibition of repression by TSA+NAM (Figure 8). These data indicate that deacetylation of Gfi1 is required for *Runx2* repression. Gfi1 is known to bind histone deacetylases (HDACs), and we have shown by ChIP that Gfi1 recruits HDAC1 to the *Runx2* promoter. The LIM domain protein Ajuba had been reported to bind Gfi1 and form the ternary complex Gfi1-Ajuba-HDAC1 that results in HDAC1-dependent repression of a

subset of Gfi1 target genes. Since Ajuba can also shuttle between the cytoplasm and nucleus, and we have shown that Gfi1 is induced to shift from the cytoplasm to the nucleus in MC4 cells by MM cells, TNFα, and IL-7, we hypothesized that Ajuba might cooperate with Gfi1 to repress *Runx2*.

We first confirmed our original western blot data of cell fractions that MM cells induce Gfi1 translocation from the cytoplasm to the nucleus using confocal microscopy and fluorescent-antibodies to study the cellular localization of endogenous Gfi1 protein in MC4 cells before and after MM cell exposure (Figure 9). Interestingly, in the unexposed MC4 cells, the large majority of Gfi1 was clearly not in the nucleus (Figure 9) and, instead, co-localized with an ER marker (Grp78BIP) (Figure 10). MM cell exposure for 48 hours induced the translocation of Gfi1 into the nucleus (Figure 9). As demonstrated in Figure 11, Gfi1 co-transfection with a *Runx2*-Luc reporter inhibits the *Runx2* promoter in a dose-dependent manner. Therefore, we selected a suboptimal dose of Gfi1 to co-transfect with an increasing amount of Ajuba expression plasmid. These studies revealed that Ajuba potentiated dose-dependently Gfi1 repression of the *Runx2* promoter (Figure 12). We compared the ability of full-length Ajuba to potentiate Gfi1 with the function of the Ajuba PreLIM domain and the LIM region domain (Figure 13). The isolated LIM region domain was competent to potentiate Gfi1 repression of *Runx2*, whereas, the isolated PreLIM domain was not. As expected, ectopically expressed Myc-Ajuba and Flag-Gfi1 interact as detected by a co-immunoprecipitation (IP) assay (not shown). Analysis of Ajuba protein levels in MC4 cells before and after MM cell exposure revealed that, like Gfi1, Ajuba protein is upregulated by MM cell exposure (not shown).

We assessed a set of Ajuba shRNAs and determined that #7552 (ShAjuba52) knocked down Ajuba RNA and protein to ~36 percent (Figure 14). Co-transfection of Gfi1 and *Runx2*-Luc into MC4 cells stably transfected with shAjuba52 revealed that ectopic Gfi1 requires endogenous Ajuba to repress the *Runx2* promoter (Figure 15), and ChIP assays demonstrated that loss of Ajuba impaired ectopic Gfi1 binding to the endogenous *Runx2* promoter in MC4 cells (Figure 16). Further, co-transfection of Gfi1 and Ajuba into MC4 cells increased ectopic Gfi1 binding to the endogenous *Runx2* promoter (Figure 17). Gfi1 biotin-oligo pulldown using programmed HEK293 extracts revealed that Ajuba interacts with Gfi1 on *Runx2* promoter DNA (Figure 18). Importantly, Ajuba was detected by ChIP on the amplicon of the endogenous *Runx2* gene where Gfi1 binds (Figure 19), indicating that Gfi1 brings Ajuba to the *Runx2* promoter. Together, these data suggest that Ajuba brings HDAC1 to Gfi1 to deacetylate it, thereby enhancing binding of the Gfi1-Ajuba-HDAC1 complex to the *Runx2* promoter, and positioning HDAC1 to deacetylate the *Runx2* promoter histones as part of the repression mechanism. Then, Gfi1 is also positioned to recruit LSD1 and CoREST to demethylate the *Runx2* promoter histones as another part of the repression mechanism. We do not yet know if Gfi1-K292R also is still potentiated by Ajuba.

In addition, we generated single and double mutants (S or T to A) of the 3 Aurora A kinase sites on Gfi1 (S216, S326, and T481) to prevent phosphorylation. We have analyzed the ability of these Gfi1 mutants to repress *Runx2* and respond to Aurora A kinase inhibition of Gfi1 repression in HEK293 cells. The effects of these mutations have been difficult to interpret: Gfi1-S216A, Gfi1-S326A, Gfi1-S216A/T418A, and Gfi1-S326A/T418A all still repress a *Runx2*-promoter reporter, whereas Gfi1-T418A and Gfi1-S216A/S326A do not (not shown). Of the Gfi1 mutants that repress the *Runx2* promoter, they all are still inhibited by over-expression of Aurora

A kinase except Gfi1-S216A/T418A (not shown). We also found that Aurora A kinase knockdown in MC4 cells increased both endogenous Gfi1 and Ajuba protein and RNA (not shown), and Aurora A kinase over-expression decreased Gfi1 and Ajuba RNA (not shown). MM cells decreased Aurora A kinase RNA in MC4 cells (not shown). The decrease of Aurora A kinase by MM treatment suggests that this effect would permit increased Gfi1 expression and function, with less phosphorylation. This observation is at odds with the ability of Aurora A kinase to increase Gfi1 protein stability by phosphorylation that we observed in HEK293 cells.

In summary, we have begun to understand some of the protein modifications and interactions that regulate Gfi1 repression of the *Runx2* gene to suppress osteoblast differentiation.

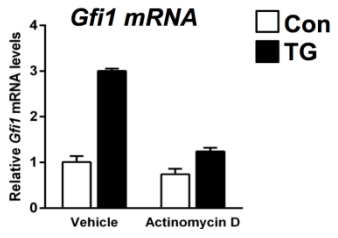

Figure 1. Gfi1 upregulation by the ER stress inducer thapsigargin (TG) is blocked by actinomycin D.

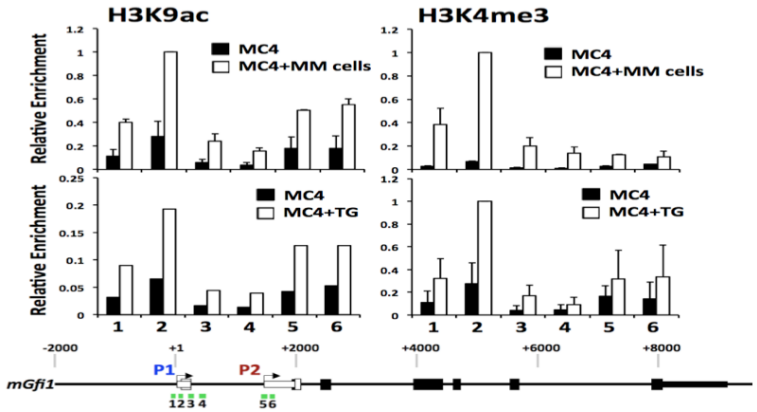

Figure 2. Both MM cell exposure and TG treatment of MC4 cells induce acquisition of histone marks indicative of *Gfi1* gene activity. MC4 cells alone or co-cultured with MM cells (48 h) or treated with TG (6 h) were subjected to ChIP for H3K9ac and H3K4me3. Amplicons assessed in *Gfi1* promoters P1 and P2 are diagrammed. Within an experiment, the data were calculated based on amplicon 2 MC4+MM cells as a reference. The averages of two (TG) or three (MM) independent biological replicates were plotted.

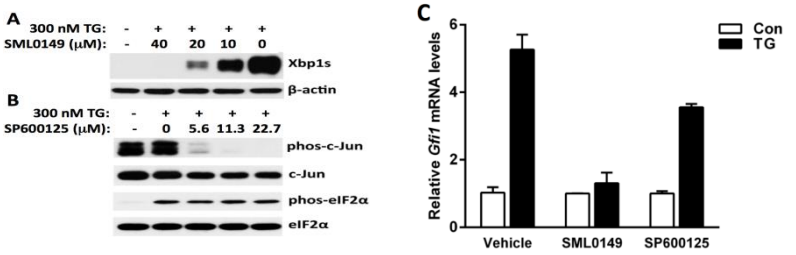

Figure 3. Inhibition of Ire1α RNase blocked TG upregulation of *Gfi1*. (A) TG (6h) treatment of MC4 cells pretreated with Ire1α RNase inhibitor (SML0149; μM as shown). (B) MC4 cells were pretreated with JNK inhibitor (SP600125; μM as indicated) before TG treatment (1h). (A,B) Cell lysates were immunoblotted as indicated. (C) qPCR showing TG (6h) induction of *Gfi1* mRNA in cells pretreated with SML0149 (40 μM) or SP600125 (22.7 μM).

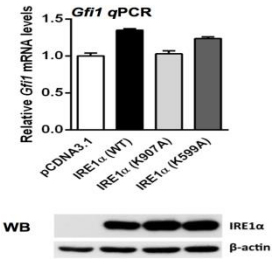

Figure 4. Up-regulation of *Gfi1* mRNA is mediated by Ire1α RNase activity. MC4 cells transfected with empty vector (pCDNA3.1), hIRE1α (WT), RNase-deficient (K907A), or kinase-deficient (K599A). *Gfi1* mRNA levels were measured by qPCR. Protein lysates were analyzed for the ectopic hIRE1α by WB.

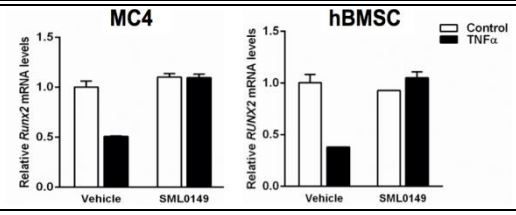

Figure 5. Inhibition of Ire1α RNAse activity blocked down-regulation of *Runx2* mRNA by TNFα. Either MC4 cells or human BMSCs (hBMSC) were pretreated with 40 μM SML0149 before treatment with 1 ng/mL TNFα for 6 hrs. Total RNAs were analyzed by qPCR for mouse *Runx2* (left panel) or human *RUNX2* (right panel) mRNA expression.

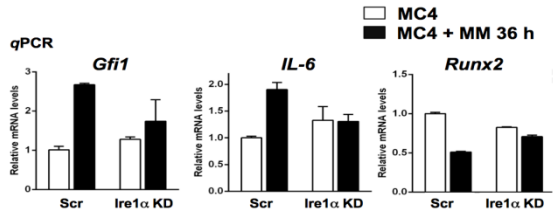

Figure 6. Knockdown of *Ire1α* in MC4 cells blocked the MM cells' repression of *Runx2*. (A) Cells transfected with scrambled control (Scr) or *Ire1α* siRNA (*Ire1α* KD) were co-cultured with MM cells in a transwell. After 36 hours, total RNA was extracted and analyzed for the expression levels of *Gfi1*, *Runx2*, and *IL-6* mRNA. The reference sample for each gene set is the "Scr siRNA with no MM cells."

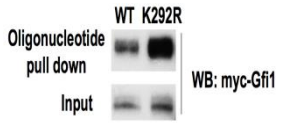

Figure 7. Gfi1 biotin-oligo pulldown using Gfi1-WT and Gfi1-K292R transfected HEK cell lysates.

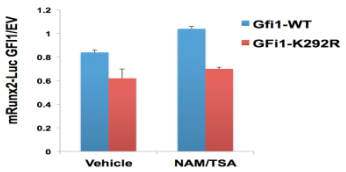

Figure 8. Co-transfection of Gfi1-WT and Gfi1-K292R with Runx2-Luc with vehicle or NAM/TSA deacetylase treatment.

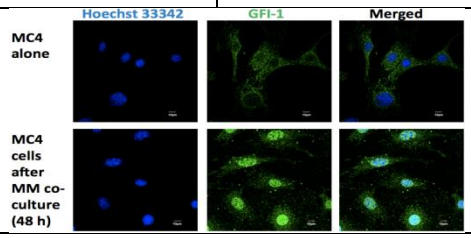

Figure 9. Confocal imaging of endogenous Gfi1 localization in MC4 cells before and after MM exposure. Hoechst 33342 stains the nuclei.

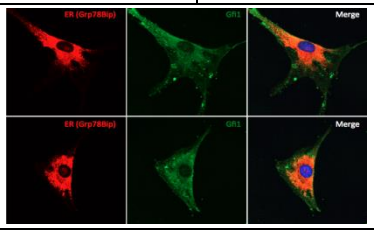

Figure 10. Confocal imaging of endogenous Gfi1 in untreated MC4 cells along with a marker of the ER (anti Grp78BIP) and Hoechst 33342 reveals Gfi1 is in the ER.

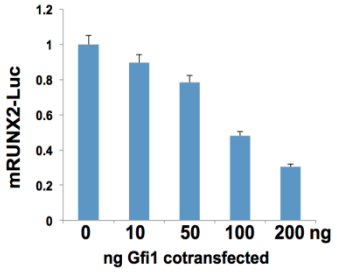

Figure 11. Cotransfected Gfi1 expression plasmid (Gfi1-pcDNA3.1) repressed -976/+110 *Runx2* promoter activity driving luciferase expression in a dose-dependent manner in MC4 cells.

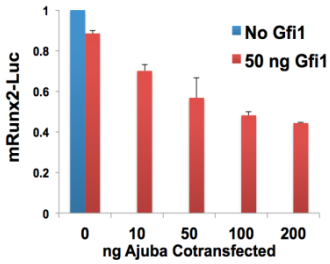

Figure 12. Cotransfected Ajuba (in a dose-dependent manner) can potentiate a suboptimal level of Gfi1-pcDNA3.1 to repress *Runx2* promoter activity.

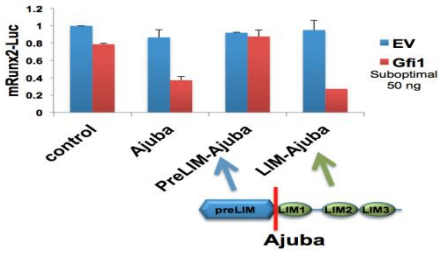

Figure 13. Full-length, preLim-Ajuba, and LIM-Ajuba cotransfected with suboptimal Gfi1-pcDNA3.1and *Runx2*-Luc reporter (MC4 cells) demonstrate that the Ajuba LIM domain region is required to potentiate Gfi1 repression of the *Runx2* promoter.

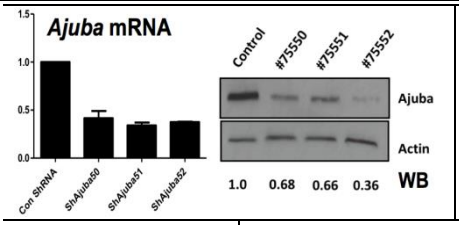

Figure 14. Ajuba shRNA 7552 most effectively knocks down Ajuba mRNA and protein.

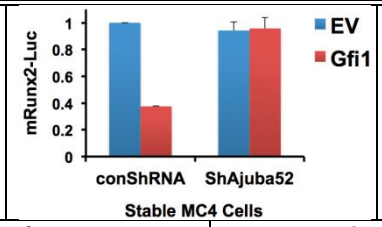

Figure 15. Ectopic Gfi1 requires Ajuba to repress the Runx2 promoter. Gfi1-pcDNA3.1 was cotransfected with *Runx2*-Luc into MC4 cells stably transfected with control ShRNA or ShAjuba52.

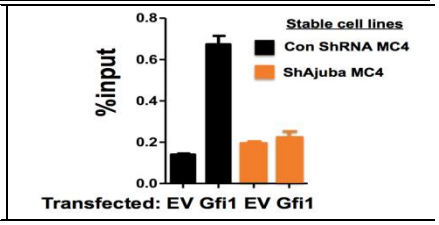

Figure 16. ChIP assay revealed that Ajuba knockdown impaired ectopic Gfi1 binding to the endogenous Runx2 promoter. Flag-mGfi1 and Flag-EV were transfected (48 h) into ConShRNA or ShAjuba MC4 stable cells. The chromatin used for ChIP with IgG and anti-Flag antibodies, Amplicon: -111/+123 *Runx2*.

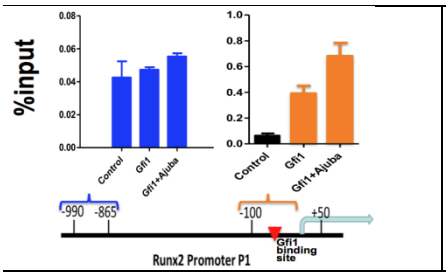

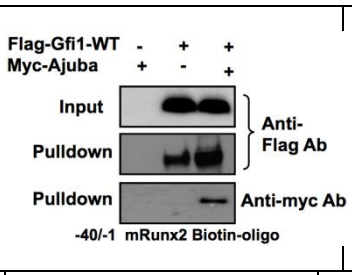

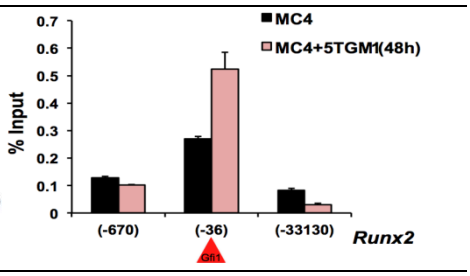

Figure 17. Ajuba increases Gfi1 binding to *Runx2*. MC4 cells transfected with Flag-mGfi1 with and without Myc-Ajuba were incubated for 48 h and then the cells were subjected to ChIP with IgG or anti-Flag Abs. Amplicons: -990/-865 (no Gfi1 site) and -111/+123 (Gfi1 site at -21/-16). Amplicon midpoints indicated.

Figure 18. Ajuba interacts with Gfi1 on DNA. Lysates from HEK293 cells transfected with Myc-Ajuba, Flag-Gfi1 or both were used in a biotin-oligo pulldown and analyzed as indicated.

Figure 19. Ajuba is present on the *Runx2* gene within the Gfi1 binding site amplicon. MC4 cells, untreated or co-cultured with 5TGM1 MM cells (48h), were subjected to ChIP analysis for endogenous Ajuba binding to the endogenous *Runx2* promoter (biological duplicates). The -36 amplicon detects Gfi1 binding at -21/-16.

Research Project 12: Project Title and Purpose

Analysis of Hsp90 and Oct3/4 Function in Radiation-induced Stemness in NSCLC – Radiotherapy for patients with non-small cell lung carcinoma (NSCLC) remains largely palliative due to resistance, which is thought to be associated with the existence of cancer stem cells (CSCs). This project is designed to answer fundamental radiobiological questions and generate new knowledge regarding lung CSC biology and the role of the molecular chaperone heat shock protein 90 (Hsp90) and the pluripotency gene octamer binding transcription factor 3/4 (Oct3/4) in radiation-induced stemness. Results of this project may lead to the development of new treatment approaches in NSCLC.

Anticipated Duration of Project

7/19/2013 - 12/31/2014

Project Overview

Radiotherapy for patients with non-small cell lung carcinoma (NSCLC) remains largely palliative due to resistance, which is thought to be associated with the existence of cancer stem cells (CSCs). In addition to pre-existing CSCs, epithelial-to-mesenchymal transition (EMT) leads to the *de novo* development of stem cell-like cells that may constitute an important mechanism of radiation resistance. Octamer binding transcription factor 3/4 (Oct3/4) plays a key role in embryonic stem cell and CSC self-renewal and pluripotency. The molecular chaperone heat shock protein 90 (Hsp90) regulates the conformation, function, and activation of a number of client proteins involved in the control of pivotal cellular functions, including known inducers and regulators of EMT in tumor cells. Blocking Hsp90 initiates client protein degradation.

We hypothesize that: (1) radiation treatment of NSCLC cells induces EMT and stem cell traits in heterogeneous cancer cells via upregulation of the pluripotency gene Oct3/4; and (2) Oct3/4 is a

client protein for molecular chaperone Hsp90 and, therefore, Hsp90 inhibition will abrogate generation of CSCs and increase efficacy of radiation treatment in NSCLC.

We will use primary human bulk NSCLC cell cultures recently established from surgical tumor samples to test our hypotheses through the following specific aims:
Aim 1. Analyze the role of Hsp90 in EMT, investigate the molecular mechanism of radiation-induced EMT, and determine whether Hsp90 inhibition blocks EMT activation in NSCLC cells.
Aim 2. Investigate radiation-induced Oct3/4 activation; analyze the role of intracellular Hsp90 in regulating lung cancer stem cell pluripotency and its underlying mechanism, and determine whether radiation-induced stemness in NSCLC is mediated by EMT mechanisms.

The successful completion of our proposed aims will generate new knowledge about NSCLC biology and the role of Hsp90 and Oct3/4 in radiation-induced stemness and EMT mechanisms, which may lead to significant improvements in the efficacy of NSCLC radiation therapy.

Principal Investigator

Vera Levina, PhD
Research Assistant Professor
Department of Medicine, Hematology/Oncology Division
University of Pittsburgh School of Medicine
Hillman Cancer Center, Suite 1.19c
5117 Center Avenue
Pittsburgh, PA 15213

Other Participating Researchers

Chitralekha Bhattacharya, PhD; Roberto Gomez-Casal, MS – employed by University of Pittsburgh

Expected Research Outcomes and Benefits

The epithelial-to-mesenchymal transition (EMT) of tumor cells may constitute an important mechanism of radiation resistance in non-small cell lung carcinoma (NSCLC). Ionizing radiation (IR) is used for 40 percent of patients with unresectable NSCLC tumors; however, radiotherapy remains largely palliative due to radioresistance. Currently, little is known about the mechanisms of EMT in NSCLC cells compared with other solid tumor cells. The study of human NSCLC is restricted in part due to the complexity of the disease and cellular heterogeneity. Therefore, to move NSCLC therapy toward personalized medicine with prospective diagnosis and effective therapies, a closer examination of EMT and IR-induced stemness is required.

Our project aims to characterize the role of the molecular chaperone heat shock protein 90 (Hsp90) and pluripotency gene octamer binding transcription factor 3/4 (Oct3/4) in radiation-induced stemness and EMT mechanisms in NSCLC. Our preliminary data demonstrate that the Hsp90 inhibitor ganetespib abrogates growth of radioresistant NSCLC cells. This project will

further characterize the role of Hsp90 in radiation resistance of NSCLC. We expect to identify novel therapeutic avenues, including the conceptually innovative strategy of combining IR to eliminate bulk tumor cells, with Hsp90 inhibition to prevent EMT and eliminate cancer stem cells within NSCLC tumors.

Summary of Research Completed

During the reporting period, progress was made toward the main objectives of this research project, as outlined below.

Aim 1. Analyze the role of Hsp90 in EMT, investigate the molecular mechanism of radiation-induced EMT, and determine whether Hsp90 inhibition blocks EMT activation in NSCLC cells

KRAS mutant NSCLC cells are the most resistant to chemotherapy and radiotherapy. Currently, there is no effective targeted therapy against KRAS mutant NSCLC. Therefore, in our study we focus specifically on KRAS mutant adenocarcinoma cells. We use an A549 cell line that was obtained from the American Type Culture Collection (ATCC) and two primary NSCLC cell lines, T2821 and T2851, that we recently established from surgical tumor samples provided through the University of Pittsburgh Cancer Institute (UPCI) Lung Cancer Specialized Program of Research Excellence (SPORE). These samples were identified as adenocarcinoma histological subtypes with KRAS mutation in codon 12 (Table 1). We found that Hsp90 is expressed in ionizing radiation (IR)-treated KRAS mutant NSCLC cells, suggesting that Hsp90 can serve as a target for improving NSCLC therapy (Figure 1, data shown for T2821 cells). Using quantitative real-time PCR (qPCR), we demonstrated that IR treatment of KRAS mutant cells, growing in stem-cell selective conditions as tumor spheres, leads to a dramatic upregulation of pluripotential embryonic transcription factor Oct3/4 gene expression (Figure 2, data shown for A549 cells). This activation of Oct3/4 expression was associated with dramatic upregulation of Hsp90 (*HSP90AA1*) gene expression (data not shown).

Recently, we have reported that IR treatment of NSCLC cells leads to the activation of epithelial-mesenchymal transition (EMT) and cancer stem cell (CSC) phenotypes in radiation resistant residual NSCLC cells that were able to survive after IR treatment. Here, we have tested whether the Hsp90 inhibitor ganetespib is able to inhibit the activation of EMT and CSC phenotypes in NSCLC cells. We analyzed the levels of protein and gene (mRNA) expression of two major transcription factors regulating EMT transition, SNAIL1 and TWIST1, and stem cell transcription factor Oct3/4. Ganetespib dramatically down-regulated levels of TWIST and SNAIL gene expression (Figure 3), as well as Oct3/4 gene expression (Figure 4), as shown by qPCR. As mRNA levels were decreased, levels of SNAIL, TWIST, and Oct3/4 proteins were also significantly down-regulated in ganetespib-treated cells (data not shown). These data support the idea that targeting Hsp90 may potentiate the effects of ionizing radiation against KRAS mutant NSCLC.

We then tested the effect of combining IR and ganetespib treatment on NSCLC cells *in vitro*. Using a clonogenic survival assay, we showed that ganetespib dramatically increases the radiosensitivity of KRAS mutant NSCLC cells, and the inhibitory effect of ganetespib is concentration-dependent (Figure 5, Table 2). The significant reduction of the clonogenic survival

of irradiated T2821, T2851, and A549 cells was observed even when ganetespib was applied at such a low concentration as 3 nM or 4 nM (Figure 5). The statistical analysis of the clonogenic survival data performed, using linear quadratic and single-hit multi-target models, confirmed that ganetespib significantly sensitizes NSCLC cells to IR treatment (Table 2).

Aim 2. Investigate radiation-induced Oct3/4 activation; analyze the role of intracellular Hsp90 in regulating lung cancer stem cell pluripotency and its underlying mechanism, and determine whether radiation-induced stemness in NSCLC is mediated by EMT mechanisms.

We confirmed that the Hsp90 inhibitor ganetespib is able to abrogate radiation-induced stemness. Using flow cytometry fluorescently activated cell sorting (FACS) for CD133-negative, CD117-negative, and CD166-negative cells, we depleted the NSCLC population for lung CSCs. These purified non-CSCs were plated and pretreated (or not treated) with ganetespib (25 nM) for 24 hours, then irradiated (0-10 Gy) and replated into ultralow attachment plates with serum-free stem cell selective media supplemented with growth factors. We found that IR-treated cells that were not treated with ganetespib generated CSCs growing as tumor spheres. NSCLC cells that were pretreated with the Hsp90 inhibitor did not have any growing tumor spheres. Next, we tested whether tumor spheres that were already generated could be inhibited or completely eliminated with ganetespib. As shown in Figure 6, ganetespib effectively inhibited T2821 and T2851 CSCs tumor spheres (Figure 6). These data indicate that the Hsp90 inhibitor is an effective tool against lung CSCs generated by IR treatment.

To further clarify the role of Oct3/4 in NSCLC cells, we generated stable cells overexpressing an Oct3/4-GFP construct. These cells also co-express high levels of Hsp90. We demonstrated an up-regulation of lung cancer stem cell marker CD166 and CD44, a receptor for hyaluronic acid, in Oct3/4-GFP transfected cells (Figure 7).

In summary, our results over the past year support the idea that CSCs constitute an important component in resistance to IR therapy in NSCLC. The transcription factor Oct3/4 is a key player for IR-induced stemness. Oct3/4 is a client protein for molecular chaperone Hsp90; therefore, targeting Hsp90 activity with ganetespib may reduce or eliminate lung CSCs and potentiate the effects of IR therapy in NSCLC.

Table 1. NSCLC Sources for Primary Adenocarcinoma Cell Cultures

#	TNM stage	Tumor	Primary Tumor?	Mutations			
				KRAS	BRAF	EGFR	EML4 /ALK
T2821	F/54	IV (T4Nx)	second, T2N1	Yes, Codon12	No	No	No
T2851	F/74	T2N0	Yes	Yes, Codon12	No	Yes, exon 21	No

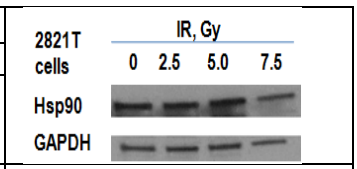

Figure 1. Hsp90 protein expression in IR treated cells. T2821 cells were irradiated and harvested after 48 h.

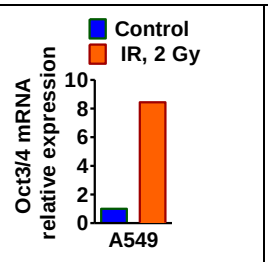

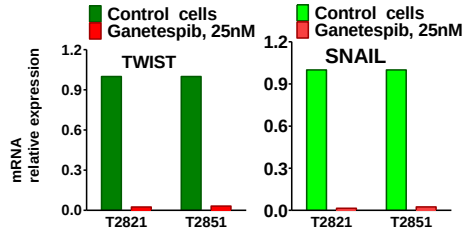

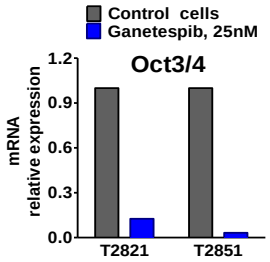

Figure 2. IR induces Oct3/4 gene upregulation. A549 tumor sphere cells were IR -treated (2 Gy), and RNA was extracted after 172 h.

Figure 3. Hsp90 inhibitor ganetespib downregulates TWIST and SNAIL mRNA expression in T2821 and T2851 primary NSCLC cells. Cells were exposed to ganetespib, 25 nM for 48h, and total RNA was extracted. TWIST and SNAIL mRNA levels were then determined by qPCR.

Figure 4. Inhibition of Hsp90 with ganetespib downregulates expression of transcription factor Oct3/4. Cells were treated with ganetespib, 25 nM for 48h, and total RNA was extracted. Oct3/4 mRNA levels in each cell line were then determined by qPCR.

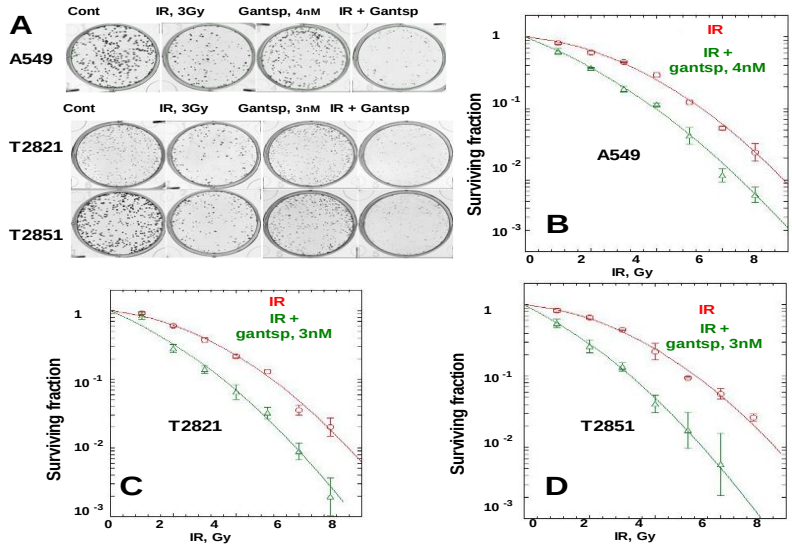

Figure 5. Clonogenic survival of NSCLC cells treated with ganetespib and IR**.** Cells were irradiated (0–10 Gy) and plated. The next day, ganetespib was added or not to the culture media. Cells were fixed after 7 days, and clonogenic survival was estimated.
(A) Representative images of cell clones generated from IR (3 Gy) treated or control cells in the presence or absence of ganetespib. Ganetespib was applied at 4 nM for A549 cells and 3 nM for T2821 and T2851 cells. (B-D) IR survival curves show IR sensitivity of A549 (B), T2821 (C) and T2851 (D) cells growing without inhibitors (red line), or growing in the presence of ganetespib (3 nM or 4 nM, green line). Average data of five experiments is presented.

Table 2. Comparison of radiosensitivity of NSCLC cells treated +/- Hsp90 inhibitor ganetespib

Cell line	T2821		T2851		A549	
Treatment	IR	IR+ ganetespib, 3nM	IR	IR+ ganetespib	IR	IR+ ganetespib
D_0 *p* (vs IR)	1.279 ± 0.12	1.047 ± 0.03 0.046	1.351 ± 0.07 -	1.285 ± 0.02 0.023	1.511 ± 0.07	1.358 ± 0.02 0.035
ñ *p* (vs IR)	5.314 ± 0.91	3.018 ± 0.26 0.026	4.901 ± 0.34 -	1.360 ± 0.34 0.003	3.830 ± 0.757	1.677 ± 0.15 0.029

Results were calculated with linear quadratic and single hit multi-target models and presented as D_0 –Gy (the dose required to reduce the fraction of survived cells to 37%) and ñ (extrapolation number derived by extension of the linear proportion of the IR survival curve to the ordinate of the graph using a log/linear plot).

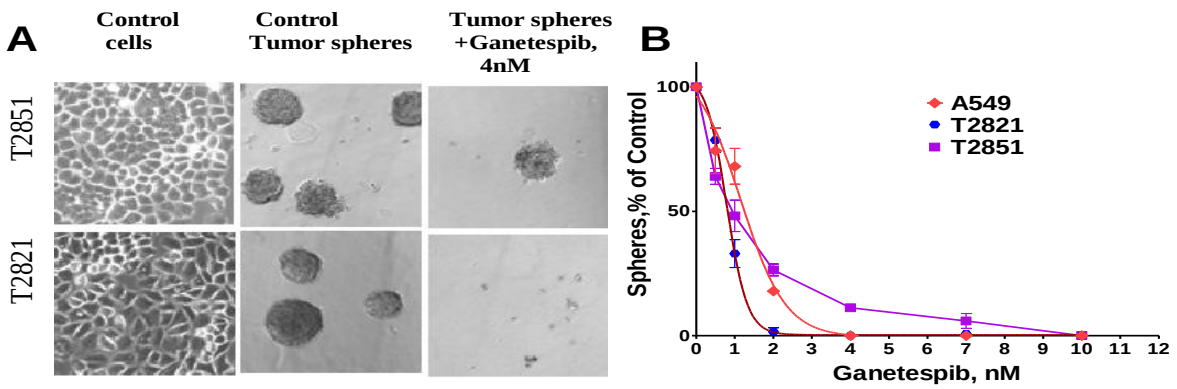

Figure 6. Hsp90 inhibitor ganetespib inhibits growth of KRAS mutant NSCLC cells growing as adherent cultures and as tumor spheres. A. Ganetespib inhibited tumor sphere growth. Representative images of control T2821 and T2851 cells cultured in adherent condition (left panel), untreated CSCs (medium panel), and CSCs treated with 4 nM of ganetespib (right panel) are shown. B. Tumor spheres were grown in serum-free media and grown in the presence of ganetespib (0-100nM) for 7 days before counting. Results are shown as % of control.

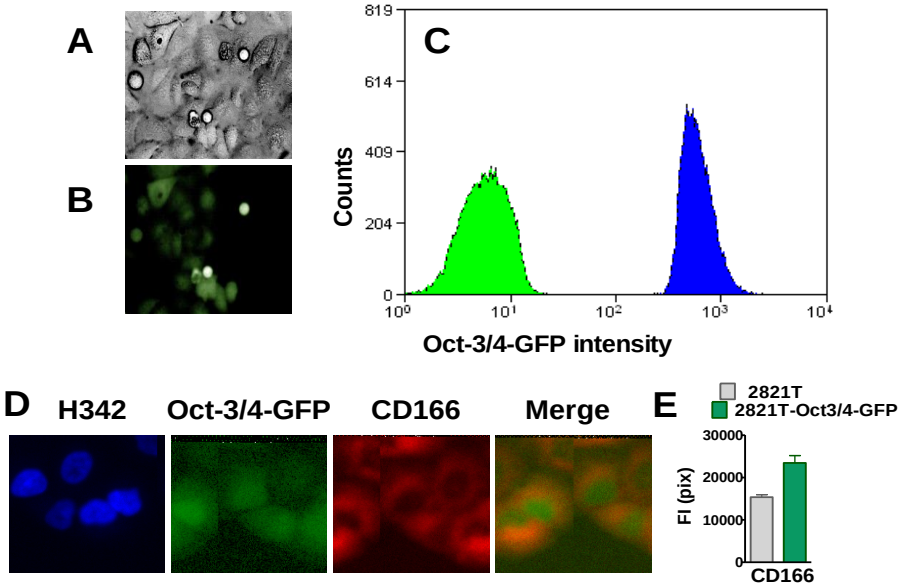

Figure 7. Characterization of Oct3/4–GFP transfected 2821T cells. 2821T cells were stably transfected with Oct3/4-GFP plasmid. A, B. The same field of cells visualized in light and fluorescent microscopy. C. GFP+ cells (approximately 1% of the entire population) were isolated by fluorescence-activated cell sorting (FACS). D. Images of T2821-Oct3/4-GFP cells stained for lung CSC marker CD166 . E. The total fluorescence intensities (FI) of CD66 in T2821cells (grey) and in T2821-Oct3/4-GFP cells (green) are shown.

Research Project 13: Project Title and Purpose

Regulation of the Estrogen Receptor in Anchorage Dependent and Independent Conditions – The estrogen receptor (ER) is a critical target in breast cancer, and a better understanding of ER action may lead to novel approaches for treatment or combating resistance to hormone therapy. Estrogen, and anti-estrogens such as fulvestrant, cause degradation of ER protein, which may subsequently limit ER activity. We have found that fulvestrant degrades ER via two specific lysine residues. In this project, we will investigate mechanisms of ER degradation using 2D and 3D cell line models to provide novel insight into therapies targeting ER in breast cancer.

Duration of Project

7/19/2013 - 6/30/2014

Project Overview

The objective of this project is to understand how estrogen receptor (ER) protein is degraded by estrogen and the anti-estrogen fulvestrant (in contrast to the anti-estrogen 4OH-tamoxifen, which stabilizes the receptor). This objective is important because ER is one of the major therapeutic targets in breast cancer, and fulvestrant may, in part, exert its action via degradation of ER. Understanding how ER is degraded may open new avenues for inhibiting ER action in breast cancer. We will examine ER degradation by estrogen and anti-estrogen in a range of breast cancer cell lines, in both two-dimensional (2D) and three-dimensional (3D) cultures. Degradation has not previously been studied in 3D and may occur via a different mechanism than in cells grown on plastic (2D). Studies in 3D will require advanced microscopy and imaging.

The specific aims of the project include:

(1) Test the effect of estrogen and anti-estrogens (fulvestrant, 4OH-tamoxifen) on degradation of ER protein in a range of breast cancer cell lines grown in 2D culture.
(2) Examine the effect of estrogen and anti-estrogens on ER degradation in breast cancer cell lines grown in 3D culture.
(3) Determine how the ER nuclear localization sequence, and mutations within this domain, affect ER localization and degradation by estrogen and anti-estrogen.

Specific Aim 1 will be completed using a range of ER-positive breast cancer cell lines (MCF7, ZR75, T47D and MDA-MB-134VI). Cells will be cultured with hormones, and ER mRNA and protein levels will be determined. ER location and levels will be visualized by immunofluorescence microscopy. All assays will be performed with time and dose responses. In Specific Aim 2, the same cell lines will be grown in 3D culture using soft agar or matrigel as a support. Cells will be stimulated with hormones, and ER levels and localization will be examined. In Specific Aim 3, site-directed mutagenesis will be used to generate ER variants that contain a deletion or point mutations in the nuclear localization sequence (NLS), and ER levels and localization by immunofluoresence and immunoblotting will be examined.

Principal Investigator

Adrian V. Lee, PhD
Professor
University of Pittsburgh
Magee-Womens Research Institute
204 Craft Avenue, Room B705
Pittsburgh, PA 15213

Other Participating Researchers

Steffi Oesterreich, PhD – employed by University of Pittsburgh

Expected Research Outcomes and Benefits

We expect to find differences in ER degradation between breast cancer cell lines, and these differences may highlight novel approaches to reducing ER levels for the treatment of breast cancer. We hypothesize that culturing cells in 3D will introduce different stresses on the breast cancer cells, which will ultimately affect the response (activation and degradation) of ER to hormones. However, degradation of ER in 3D might be a more faithful recapitulation of what is seen *in vivo*, indicating that such culture conditions will need to be used for ER-related studies. Finally, we hope to identify the region of ER that is degraded by estrogen or anti-estrogen, to develop an understanding of how degradation occurs, and identify opportunities for new drugs that will induce ER degradation in breast cancer therapy.

Summary of Research Completed

Specific Aim 1:
To understand degradation of ER in 2D, we plated a series of breast cancer cells on plastic dishes, in Dulbecco's modified Eagle's medium (DMEM)+10 percent fetal bovine serum (FBS) containing estradiol. We then changed the serum to 5 percent charcoal-stripped serum (CSS) and washed the cells for three consecutive days, three times each day, with phosphate-buffered saline (PBS). This rigorous process is necessary to decreased estrogen levels in the media and attached to the cells so that maximal estrogen response can be observed. On day 4, we treated the cells with estradiol or the anti-estrogens 4-OH-tamoxifen (tam) or ICI 182,780 (ICI) for six hours, as indicated in Figure 1A. We observed estradiol-mediated downregulation of ER by estradiol and ICI in MCF-7 and T47D cells; however, the estradiol effect was lost in MDA-MB-134 cells and attenuated in Sum44 cells, suggesting that there is a difference in ER degradation between the two main histological breast cancer subtypes, invasive lobular carcinoma (ILC) and invasive ductal carcinoma (IDC). We observed stabilization of ER with tam in all cell lines.

To understand whether the effects of estrogen and ICI on ER levels are mediated by the proteasome, we then treated the cells with ligands as described above and seen in Figure 1A and added the proteasome inhibitor MG132 (Figure 1B). Collectively, these data: (1) confirmed that degradation of ER in MCF-7 cells was mediated by the proteasome; and (2) confirmed differences between the IDC and ILC cells. Intriguingly, while the estrogen-mediated degradation of ER is lost in MDA-MB-134 cells, ER remains sensitive to ICI-mediated degradation, a finding that might be of clinical importance. And finally, we asked whether the apparent lack of estradiol-mediated degradation could be rescued by increasing concentration. We treated MDA-MB-134 cells with increasing concentrations of estradiol (10^{-9}M–10^{-6}M) (Figure 2) and confirmed total loss of degradation.

Specific Aim 2:
To compare degradation of ER between 2D and 3D cultures, we plated MCF-7 and MDA-MB-134 cells directly on plastic dishes and in Matrigel. Cells were treated in duplicate as described

above, for four hours and 16 hours. Proteins were isolated and run on sodium dodecyl sulfate-polyacrylamide gel electrophoresis (SDS-PAGE). In MCF-7 cells, the effects of estradiol, tamoxifen, and ICI on ER levels were similar in 2D and 3D culture (Figure 3, top). Likewise, in MDA-MB-134 cells, the effects of ligand were similar in 2D and 3D (Figure 3, bottom), confirming that estradiol does not alter levels of ER in these ILC cells. We then studied the ER degradation through microscopic approaches, specifically, using immunofluorescence (IF). The goal was to compare 2D and 3D degradation by IF. While we were able to confirm our immunoblot results using IF of 2D cells, we had technical problems in performing IF using cells grown in 3D. We were able to grow cells in 3D and to observe estrogen effects on three-dimensional growth (Figure 4). However, the staining of ER was problematic and of insufficient quality for imaging and quantification. We recently contacted investigators at the University of Pittsburgh Drug Discovery Institute and are now collaborating with this group, headed by Lans Taylor, PhD. We are using high-throughput imaging and analysis of cells plated in Matrigel to quantify ER degradation in 3D. These studies are ongoing.

Specific Aim 3:

Previous evidence has suggested that estrogen- and ICI 182708 (ICI)-mediated degradation of ER may be associated with nuclear to cytoplasmic shuttling. To examine this question further, we created an ER mutant that lacked the nuclear localization sequence (NLS) by deleting amino acids 250-274 (ERΔNLS) (Figure 5A). Expression of the GFP-mutant ER showed that it was mainly localized in the cytoplasm (Figure 5B). As a control, we replaced the endogenous ER NLS, but on the N-terminus of ER (to determine whether location within the ER is critical). This mutant (ERΔNLS/endog-NLS) was again nuclear, showing that the NLS is functional even when placed on the N-terminus (Figure 5B). Examination of protein levels by immunoblot (Figure 5C) showed that the ERΔNLS was degraded by E2 (1nM), but degradation was resistant to ICI. Interestingly, replacement of the endogenous NLS caused ERΔNLS/endog-NLS to become sensitive to ICI-mediated degradation once more. This finding indicates that the NLS is both necessary and sufficient for degradation. As the general deletion of the NLS likely causes major changes in protein structure, we also performed site-directed mutagenesis of specific amino acids. We focused on lysine residues, which can be post-translationally modified by both ubiquitination and sumoylation. We mutated the five lysine residues to arginine and expressed this mutant (KR) (Figure 6A). While this mutant remained nuclear, i.e., the NLS was clearly active, the mutant ER (KR) was partially resistant to ICI-mediated degradation (Figure 6B).

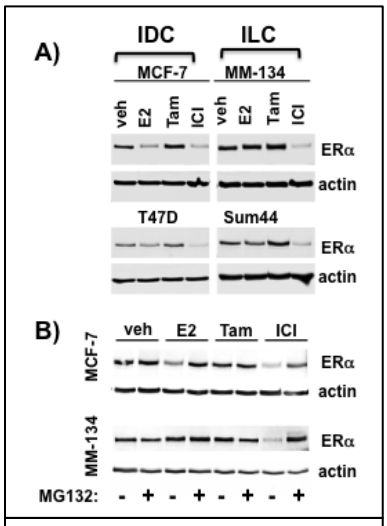

Figure 1: Degradation of ER-alpha (ER) in 2D culture. A) Breast cancer cells representing invasive ductal carcinoma (IDC) (MCF-7 and T47D) and invasive lobular carcinoma (ILC) (MDA-MB-134 and Sum44) were kept in charcoal-stripped serum (CSS) for 3 days, and then treated with 10^{-9}M estradiol (E2), 10^{-6} M 4-hydroxy-tamoxifen (tam), or 10^{-6}M ICI 182,780 (ICI). B) MCF-7 (IDC) and MDA-MB-134 (ILC) cells were treated with E2 (10^{-9}M) -/+ the proteasome inhibitor MG132 (5uM).

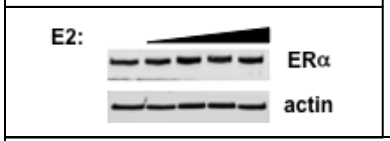

Figure 2: Lack of degradation in MDA-MB-134 cells. MDA-MB-134 cells were treated with increasing concentration of E2 for 6 hrs (10^{-9}M-10^{-6}M).

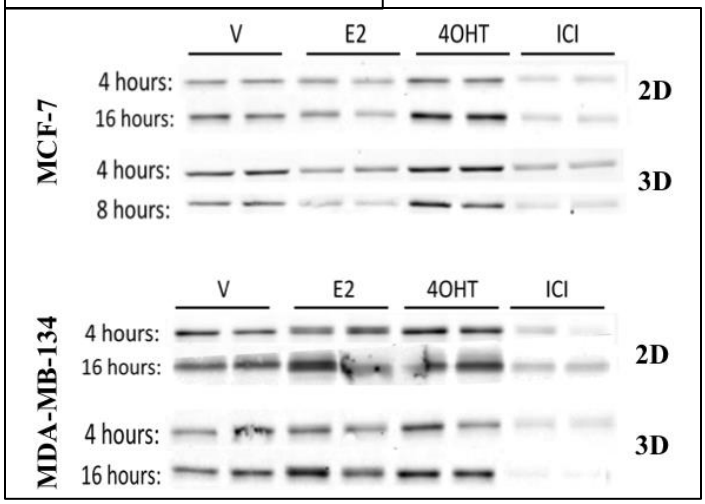

Figure 3: Comparison of ER degradation between 2D and 3D cultures. Cells were kept in CSS on plastic (2D) or in Matrigel (3D). Treatment (ligand and time) and cell lines were as indicated.

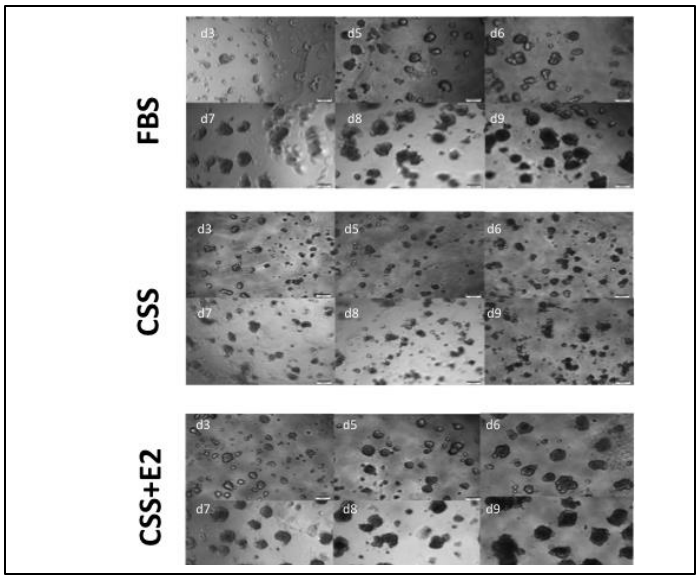

Figure 4: 3D growth of MCF-7 cells in absence and presence of estradiol. The plates were coated with 100% Matrigel, and the cells were then seeded on top in media containing 2% Matrigel.

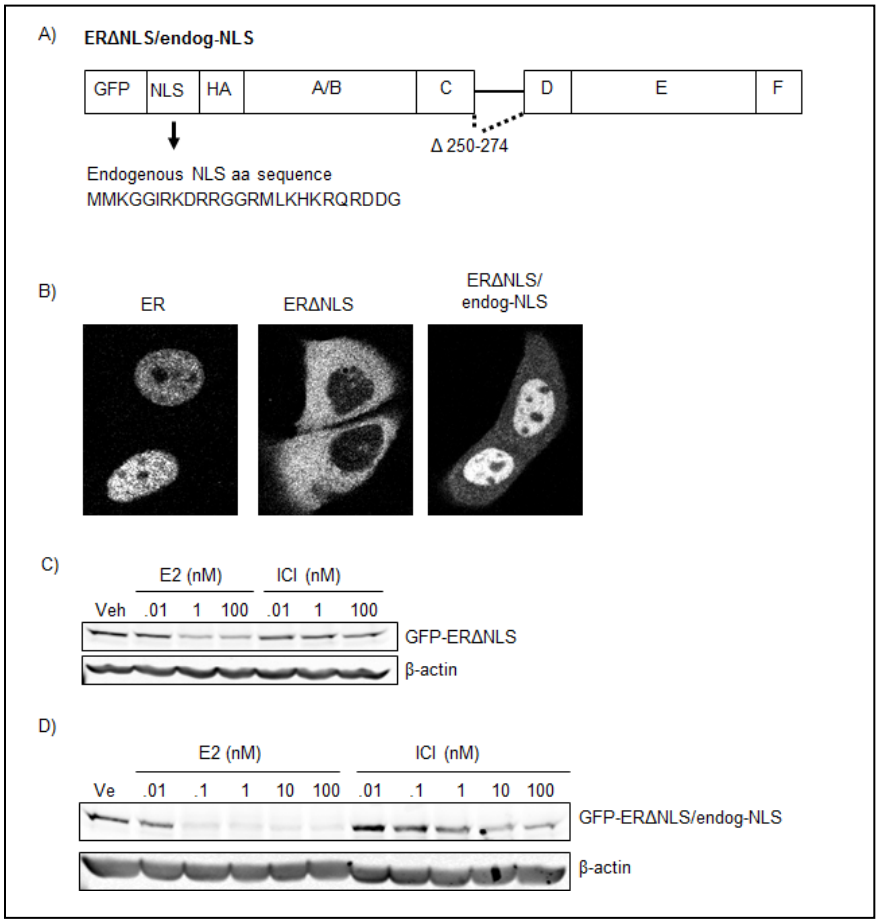

Figure 5: The nuclear localization sequence (NLS) of ER is both required and sufficient for fulvestrant-, but not estradiol-mediated degradation. (A) Schematic representation of GFP-ERΔNLS with the ERα endogenous NLS (GFP-ERΔNLS/endog-NLS) cloned near the protein's N-terminus. The endogenous ERα NLS amino acid sequence is included as one-letter abbreviations. (B) C4-12 cells transiently transfected with GFP-ER, GFP-ERΔNLS, or GFP-ERΔNLS/endog-NLS were fixed, permeabilized, and stained with an antibody directed against HA (ERα). (C, D) C4-12 cells stably expressing GFP-ERΔNLS (C) or GFP-ERΔNLS/endog-NLS (D) were treated with increasing concentrations of E2 or ICI for 24hr. Vehicle (Veh) control samples were treated with 100% ethanol. Cells were lysed and ERα protein detected by immunoblot.

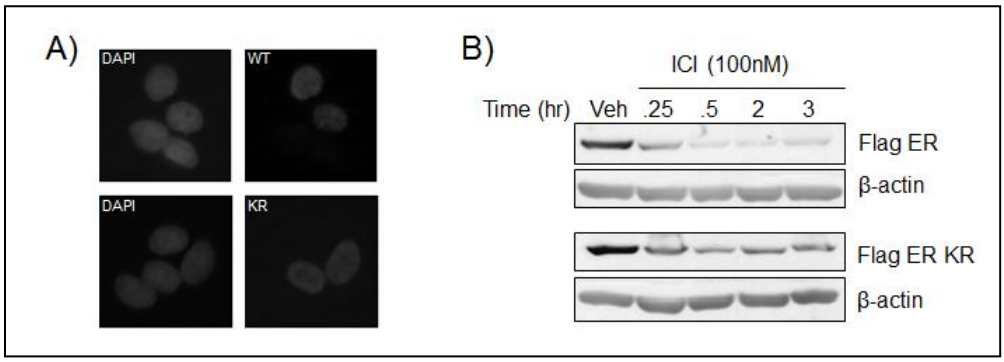

Figure 6: Point mutations of lysines in the NLS of ER blocks ICI-mediated degradation. (A) MCF-7 cells transiently expressing Flag-ERα or Flag ERα KR. Representative cells are shown. (B) HEK293 cells transiently expressing Flag-ERα or Flag ERα KR were treated with ICI at different time points. Vehicle control samples treated with 100% ethanol. Cells were lysed and ERα protein detected by immunoblot.

Research Project 14: Project Title and Purpose

Research Infrastructure: Biomedical Science Tower (BST) Animal Facility Caging Upgrade – The specific aim of this project is to improve the capacity and quality of the vivarium on the 9th floor of the Biomedical Science Tower. Capacity and quality will be expanded by reconfiguring three undersized rodent holding rooms totaling 561 net square feet, currently at our exceeding capacity, to create two larger holding rooms, both designed to accept high-density rotary individually ventilated caging (IVC) systems with significantly expanded holding capacity.

Anticipated Duration of Project

7/22/2013 - 12/31/2015

Project Overview

The BST's space allocation for animal caging is currently limited due to room size and design. Holding rooms E930, E932, and E933 will be reconfigured into two rooms, and 18 high-density racks from Animal Care Systems will be purchased and installed, increasing capacity by 67 percent, from 1,080 to 1,800 cages. These high-density rotary individually ventilated cages (IVC) have been selected because they produce low-velocity ventilation, minimizing stress to the animals. Air is filtered into and out of the cage, assuring adequate biological barriers to protect the animals and safeguard occupational health. Existing linear IVC racks that are not reused within this space will be transferred to another facility within the program that uses comparable equipment, thus expanding caging resources at that site.

The specific aim of this project is to improve the capacity and quality of the vivarium on the 9th floor of the BST. Capacity and quality will be expanded by reconfiguring three undersized rodent holding rooms totaling 561 net square feet to create two larger holding rooms, both

designed to accept high-density rotary individually ventilated caging (IVC) systems with significantly expanded holding capacity.

Principal Investigator

Arthur S. Levine, MD
Senior Vice Chancellor for the Health Sciences
John and Gertrude Petersen Dean of Medicine
Professor of Medicine and of Molecular Genetics
University of Pittsburgh
3550 Terrace Street
Suite 401, Scaife Hall
Pittsburgh, PA 15261

Other Participating Researchers

None

Expected Research Outcomes and Benefits

Installing the new caging system will increase the animal cage capacity. The new caging layout will also improve employee ergonomics by creating a clear path within each holding room between entry and exit doors and by providing adequate clearance around both new and existing caging and transfer stations, allowing staff to work safely and efficiently. Unlike the existing caging, the new IVCs are directly exhausted through the building's HVAC system, reducing staff exposure to animal dander. The proposed IVC caging system requires a low air change rate that will not increase HVAC demand and does not use motorized blowers like the existing IVCs. Thus, noise and vibration associated with such blowers will be reduced.

Summary of Research Completed

Architectural drawings for the project were completed and approved in April 2014. Bids were solicited and contracts were awarded to relevant subcontractors. Work on Phase I of the project, involving renovations to ceilings, walls, ductwork, and plumbing in rooms E912-E915, began in June 2014.